

Accepted Manuscript

Evaluating the effects of fluorine on biological properties and metabolic stability of some antitubulin 3-substituted 7-phenyl-pyrroloquinolinones

Roberta Bortolozzi, Davide Carta, Matteo Dal Prà, Giuseppe Antoniazzi, Elena Mattiuzzo, Mattia Sturlese, Veronica Di Paolo, Laura Calderan, Stefano Moro, Ernest Hamel, Luigi Quintieri, Roberto Ronca, Giampietro Viola, Maria Grazia Ferlin

PII: S0223-5234(19)30516-1

DOI: <https://doi.org/10.1016/j.ejmech.2019.05.092>

Reference: EJMECH 11402

To appear in: *European Journal of Medicinal Chemistry*

Received Date: 28 March 2019

Revised Date: 31 May 2019

Accepted Date: 31 May 2019

Please cite this article as: R. Bortolozzi, D. Carta, M.D. Prà, G. Antoniazzi, E. Mattiuzzo, M. Sturlese, V. Di Paolo, L. Calderan, S. Moro, E. Hamel, L. Quintieri, R. Ronca, G. Viola, M.G. Ferlin, Evaluating the effects of fluorine on biological properties and metabolic stability of some antitubulin 3-substituted 7-phenyl-pyrroloquinolinones, *European Journal of Medicinal Chemistry* (2019), doi: <https://doi.org/10.1016/j.ejmech.2019.05.092>.

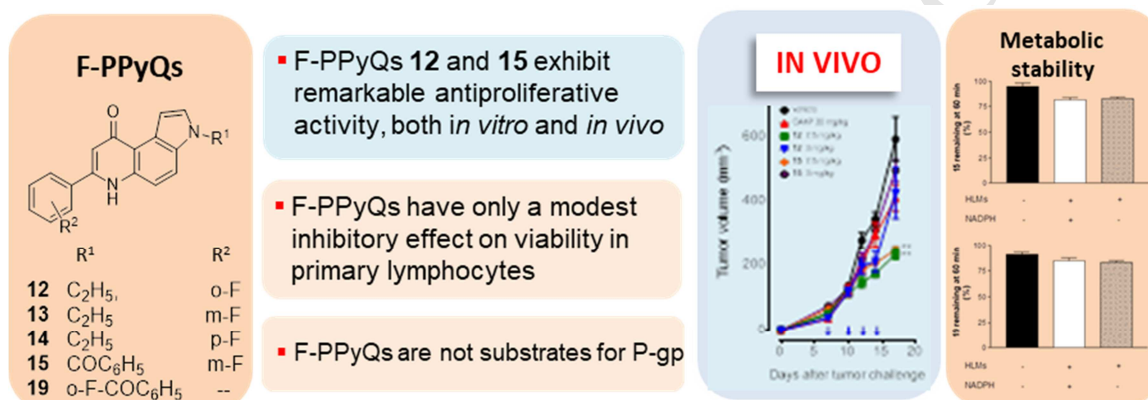
This is a PDF file of an unedited manuscript that has been accepted for publication. As a service to our customers we are providing this early version of the manuscript. The manuscript will undergo copyediting, typesetting, and review of the resulting proof before it is published in its final form. Please note that during the production process errors may be discovered which could affect the content, and all legal disclaimers that apply to the journal pertain.



GRAPHICAL ABSTRACT

Evaluating the effects of fluorine on biological properties and metabolic stability of some antitubulin 3-substituted 7-phenyl-pyrroloquinolinones

Roberta Bortolozzi, Davide Carta¹, Matteo Dal Prà, Giuseppe Antoniazzi, Elena Mattiuzzo, Mattia Sturlese, Veronica Di Paolo, Laura Calderan, Stefano Moro, Ernest Hamel, Luigi Quintieri, Roberto Ronca, Giampietro Viola, Maria Grazia Ferlin



Evaluating the effects of fluorine on biological properties and metabolic stability
of some antitubulin 3-substituted 7-phenyl-pyrroloquinolinones

Roberta Bortolozzi², Davide Carta¹, Matteo Dal Prà¹, Giuseppe Antoniazzi¹, Elena Mattiuzzo², Mattia Sturlese¹, Veronica Di Paolo¹, Laura Calderan¹, Stefano Moro¹, Ernest Hamel³, Luigi Quintieri¹, Roberto Ronca⁴, Giampietro Viola², Maria Grazia Ferlin¹

1. *Department of Pharmaceutical and Pharmacological Sciences, University of Padova, 35131 Padova, Italy.*
2. *Department of Woman's and Child's Health, University of Padova, Laboratory of Oncohematology, 35128 Padova, Italy.*
3. *Screening Technologies Branch, Developmental Therapeutics Program, Division of Cancer Treatment and Diagnosis, Frederick National Laboratory for Cancer Research, National Cancer Institute, National Institutes of Health, Frederick, Maryland 21702, USA.*
4. *Department of Molecular and Translational Medicine, Oncology and Immunology Section, University of Brescia, 29881 Brescia, Italy.*

Abstract

A small number of fluorinated 7-phenyl-pyrroloquinolinone (7-PPyQ) derivatives was synthesized in an attempt to improve the metabolic stability of 3*N*-ethyl-7-PPyQ and 3*N*-benzoyl-7-PPyQ. The possible impacts of the fluorine-hydrogen isosterism on both biological activity and metabolic stability were evaluated. Introduction of a fluorine atom in the 2 or 3 position of the 7-phenyl ring yielded the 7-PPyQ derivatives **12**, **13** and **15**, which showed potent cytotoxicity (low micromolar and sub-nanomolar GI₅₀s) both in human leukemic and solid tumor cell lines. None of them induced significant cell death in quiescent and

proliferating human lymphocytes. Moreover, **12**, **13** and **15** exhibited remarkable cytotoxic activity in the multidrug-resistant cell line CEM^{Vbl100}, suggesting that they are not substrates for P-glycoprotein. All compounds inhibited tubulin assembly and the binding of [³H]colchicine to tubulin, with the best activity occurring with compound **15**. Mechanistic studies carried out on compound **12** indicated that it caused (a) a strong G2/M arrest; (b) apoptosis in a time- and concentration-dependent manner; (c) a significant production of ROS (in good agreement with the observed mitochondrial depolarization); (d) caspase-3 and poly (ADP-ribose) polymerase activation; and (e) a decrease in the expression of anti-apoptotic proteins. *In vivo* experiments in a murine syngeneic tumor model demonstrated that compounds **12** and **15** significantly reduced tumor mass at doses four times lower than that required for the reference compound combretastatin A-4 phosphate. Neither monofluorination of the 7-phenyl ring of 3*N*-ethyl-7-PPyQ nor replacement of the benzoyl function of 3*N*-benzoyl-7-PPyQ with a 2-fluorobenzoyl moiety led to any improvement in the metabolic stability.

Keywords. Anti-tubulin, fluoro-phenylpyrroloquinolinone, apoptosis, molecular docking, structure-activity relationships, metabolic stability

1. Introduction

The introduction of fluorine atoms in organic molecule drug candidates has become a common practice in modern small-molecule drug discovery. Indeed, the presence of the small and highly electronegative fluorine is capable of modulating various molecular properties, including pharmacological potency, physicochemical features and pharmacokinetics [1]. In particular, replacement of hydrogen with fluorine in a compound subject to cytochrome P450

(CYP)-catalyzed oxidative metabolism has been frequently successful in decreasing the rate of metabolic elimination of a chemical entity, thereby improving its oral bioavailability and prolonging its *in vivo* half-life [2]. Furthermore, the substitution of fluorine in place of hydrogen has become an approach commonly used by the medicinal chemist in an attempt to improve the binding affinity of a bioactive compound to a target protein and thus, conceivably, to increase its potency and target selectivity [3-6].

Tricycle phenylpyrroloquinolinones (PPyQs) are a class of compounds that have shown interesting *in vitro* and *in vivo* antiproliferative properties acting as tubulin polymerization inhibitors by binding at the colchicine site in β -tubulin. In particular, 7-PPyQs have shown very high affinity for the colchicine site and high potency in inhibiting tubulin polymerization comparable to that of reference compounds, such as combretastatin A-4 (CA-4)[7-11]. Structural optimization efforts produced highly anti-tumorigenic PPyQs that showed nanomolar and subnanomolar GI_{50} s towards a broad spectrum of human tumor cell lines, with induction of tumor cell death by an apoptotic mechanism. These compounds also overcome resistance to taxol and vincristine, have limited cytotoxicity in non-tumor cell lines and act synergistically with conventional chemotherapeutic agents in inhibiting leukemic cell proliferation [10]. Among the synthesized compounds, 3*N*-ethyl-7-PPyQ (**20**) [9] and 3*N*-benzoyl-7-PPyQ (**21**) [11], as representative of 3*N*-alkyl and 3*N*-acyl analogues of 7-PPyQs, respectively (Figure 1), had shown the best antiproliferative profile in their respective series. In agreement with tubulin polymerization inhibition assay data, docking simulations with compounds **20** and **21** into tubulin suggested that they have a high affinity for the colchicine site (as shown for compound **21** in Figure 1) and that their binding mode is compatible with a competitive mechanism of action [11].

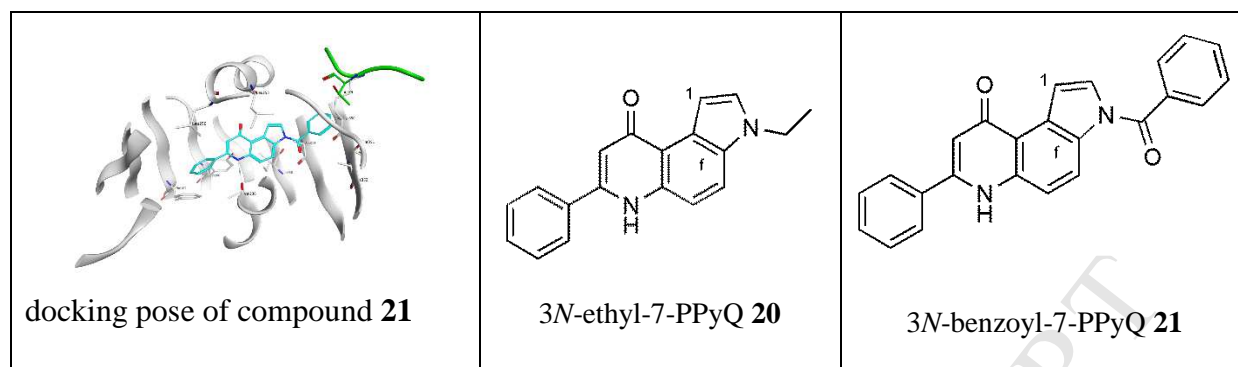


Figure 1. Molecular docking simulation of compound **21** in the colchicine site of β -tubulin and structures of 7-PPyQs **20** and **21**.

Previous *in vitro* studies in human liver microsomes (HLMs) demonstrated that the amide 3*N*-benzoyl-7-PPyQ (**21**) is quite stable to metabolism by NADPH-dependent enzymes (i.e., CYPs and flavin monooxygenases, [6]), but it was, however, susceptible to slow microsomal hydrolysis to 3*N*-unsubstituted 7-PPyQ [10]. In contrast, 3*N*-ethyl-7-PPyQ (**20**) was relatively unstable when incubated with NADPH-supplemented HLMs (0.5 mg of protein/mL), with less than 70% compound remaining after a 30-min incubation at 37°C (Di Paolo, unpublished data). Based on these findings, and in order to possibly improve the metabolic stability and anticancer properties of 7-PPyQs, we recently synthesized a small library of untargeted monofluoro-phenyl derivatives of compounds **20** and **21**. In particular, based on data from a metabolite profiling experiment indicating conversion of **20** to oxygenated metabolites by HLMs (see Results section), and, being aware that aromatic carbon oxygenation is a quite common CYP-catalyzed reaction [6] a fluorine atom was introduced in the *ortho*, *meta* or *para* position of the 7-phenyl ring of compound **20** giving compounds **12-14**. Moreover, in an attempt to further improve the stability of amide **21** to hydrolytic metabolism, we replaced its benzoyl function with a 2-fluorobenzoyl moiety, thus obtaining compound **19**. Finally, to get more insight into the possible impact of fluorination on the biological properties of PPyQs,

our library was completed with the PPyQ derivatives **15** and **18**. Since fluorination might influence both therapeutic efficacy and target affinity [5], we evaluated the synthesized fluorinated PPyQs both *in vitro* and *in vivo* by biological assays aimed at characterizing their anticancer properties. Furthermore, molecular modelling studies and metabolic stability experiments were performed with compounds **12-15** and **19**. The results of these investigations are presented and discussed in this paper.

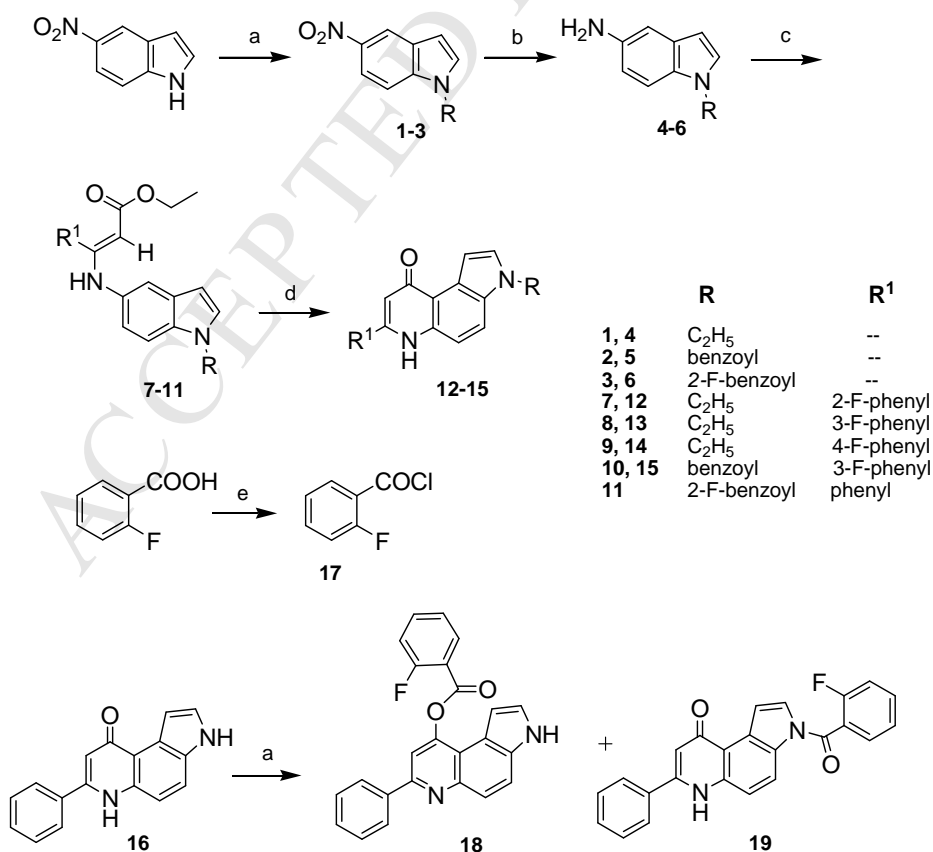
2. Results and discussion

2.1 Chemistry

The 4-step method leading to 7-PPyQ compounds was previously described [8] (Scheme 1). First, commercially available 5-nitroindole was subjected to an *N*-alkylation and acylation reactions using appropriate halogenated compounds to obtain the nitroindole derivatives **1-3**. Compound **1** was obtained using ethyl bromide in anhydrous DMF in the presence of NaH at room temperature, while for compounds **2** and **3**, a reaction with benzoyl chloride or 2-F benzoyl chloride, respectively, in presence of DMAP and pyridine at room temperature for 24 h, was preferred. The 2-fluorobenzoyl chloride (**17**) was prepared by reacting 2-fluorobenzoic acid with SOCl₂ at reflux. The catalytic reduction (Pd/C 10%, H₂ at atmospheric pressure, ethyl acetate) of intermediate **1** and (Pt/C, H₂ at atmospheric pressure, ethyl acetate) of intermediates **2** and **3** gave the corresponding aminoindoles **4-6** in almost quantitative yields. Compound **4** was reacted with commercial ethyl-2-, -3- and -4-fluoro benzoyl acetate and compound **5** with ethyl-3-fluoro-benzoyl acetate, whereas compound **6** with ethyl benzoyl acetate. All the reactions were carried out in absolute ethanol at reflux in the presence of a catalytic amount of acetic acid, yielding the acrylate derivatives as crude material **7-11**. These were purified by silica gel column chromatography before being submitted to thermal cyclization in boiling diphenyl ether (250 °C) to obtain the final products **12-15** in good

yields. Compound **11** cyclized but with loss of the 2-fluoro-benzoyl moiety, giving the known 7-PPyQ **16**.^[7] For this reason, in order to obtain the 3*N*-2-fluorobenzoyl 7-PPQ, compound **16** was directly reacted with 2-fluorobenzoyl chloride **17** in DMF in the presence of NaH, obtaining two products: the main reaction product was identified as the isomeric ester **18** (78%), and the desired 3-amide compound **19** was obtained in lower yield (22%).

Scheme 1. a) Br-ethane, NaH 60%, DMF, 50°C, 6h, 99% (**1**); benzoyl chloride, pyridine, DMAP, rt, 24h, 54% (**2**), or 2-F-benzoyl chloride, pyridine, DMAP, rt, 24h, 62% (**3**) b) H₂, Pd/C 10%, EtOAc, 50 °C, 12h, 98% (**4**) or H₂, Pt/C 15%, EtOAc, rt, 2 h, 84% (**5**, **6**); c) ethyl (2-fluorobenzoyl) acetate (**7**), ethyl (3-fluorobenzoyl) acetate (**8**, **10**), ethyl (4-fluorobenzoyl) acetate (**9**), ethyl benzoyl acetate (**11**), absolute ethanol, CH₃COOH cat, drierite, refluxing, 24-48 h, 35-70%; d) diphenyl ether, 250 °C, 15 min, 27-56%; e) SOCl₂, DCM, 80 °C, refluxing, 2 h, 80%.



2.2 Biological evaluation

2.2.1 Metabolic pattern of compound **20** in human liver microsomes

An exploratory *in vitro* drug metabolism experiment was conducted to get preliminary information on the possible metabolic fate of the known compound **20** (Figure 1) in humans. The HPLC trace of compound **20** incubated with NADPH-supplemented HLMs demonstrated three major new fluorescence peaks (Figure 2), which were undetectable when NADPH, an essential cofactor for both CYP- and flavin monooxygenase-mediated oxidations [6], was omitted from the incubation mixture (not shown). Compound **20** constituted a peak eluting at 12.9 min, while the three compound **20** metabolites (M1-M3) eluted at 11.2, 12.3 and 14.7 min, respectively; the retention time of M1 corresponded exactly to that of authentic 3*N*-unsubstituted 7-PPyQ (scheme 1, compound **16**), a recently identified metabolite arising from hydrolysis of 3*N*-benzoyl-7-PPyQ (compound **21**) catalyzed by HLMs [11]. Fractions corresponding to the M1-M3 and compound **20** peaks were collected and subjected to positive ion ESI-mass spectrometry analysis. As expected, the mass spectrum of peak M1 was compatible with that of authentic 7-PPyQ **16** and showed a prominent protonated molecule ion, $[M+H]^+$, at m/z 261.0996. These findings demonstrated that compound **20** underwent oxidative *N*-demethylation catalyzed by a human liver microsomal enzyme(s) to form 7-PPyQ. The material in peak M2 showed a $[M+H]^+$ at m/z 277.0930, which was 12.0419 Da lower than that of protonated parent compound **20** (measured m/z = 289.1349). This finding suggested the loss of C₂H₄ and the introduction of an oxygen atom into the parent molecule, i.e., deethylation and oxygenation of compound **20**. Finally, the mass spectrum scan of the most prominent chromatographic peak, M3, showed a $[M+H]^+$ ion at m/z 305.1273, which

was 15.9924 Da higher than that of **20**, suggesting that an oxygen atom has been introduced into the parent drug (oxygenation of compound **20**).

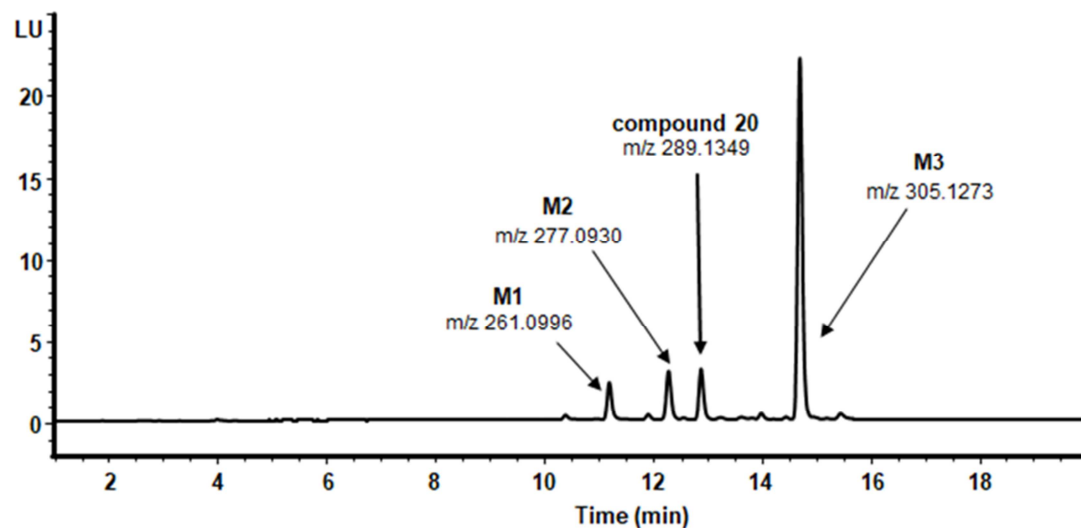


Figure 2. HPLC separation of compound **20** and its human liver microsomal metabolites **M1-M3**. HLMs (0.25 mg/mL) were incubated with 10 μ M compound **20** and NADPH (1 mM) at 37 $^{\circ}$ C for 60 min. The sample was processed and analyzed by HPLC-fluorescence as described in Materials and Methods. A peak of unmodified compound **20** and three major peaks corresponding to metabolites M1-M3 are present. All metabolite peaks were absent when NADPH was omitted from the reaction mixture. The reported m/z values were obtained from ESI-mass spectra of collected peaks and refer to $[M+H]^+$ ions.

2.2.2 Metabolic stability of compounds **12-15** and **19-21** in human liver microsomes

The metabolic stability in HLMs of fluorinated 7-PPyQs **12-14** was compared with that of their non-fluorinated counterpart, compound **20**. Like **20**, compounds **12-14** were quite stable when incubated with HLMs in phosphate buffer (pH 7.4) or phosphate buffer only, but time-dependently disappeared when both microsomes and NADPH were contained in the mixture

(Figure 3). In particular, the depletion half-lives in mixtures containing HLMs and NADPH were 11.4, 11.8, 10.6 and 17.3 min for **12**, **13**, **14** and **20**, respectively. Therefore, introduction of fluorine in the *ortho*, *meta* or *para* position of the 7-phenyl ring failed to decrease but instead slightly increased the metabolic lability of compound **20**. These findings may suggest that the 7-phenyl ring of compound **20** is not a site of carbon oxygenation by a NADPH-dependent enzyme(s) in HLMs. On the other hand, as stressed by Obach et al. [12], for compounds metabolized at multiple sites, as in the case of **20**, fluorination at a single site may only result in a “metabolic switching”, with no decrease in the overall rate of metabolic elimination. Moreover, introduction of fluorine at a metabolically labile site can also unexpectedly increase the rate of metabolism by CYP enzymes, as observed for substitution of fluorine in place of hydrogen at the tolyl methyl group of celecoxib or at position 2 of ramelteon [12]. Proper interpretation of the results of this set of experiments thus requires a more in-depth metabolic profiling (i.e., identification of the metabolic “hot spots”) of compound **20**.

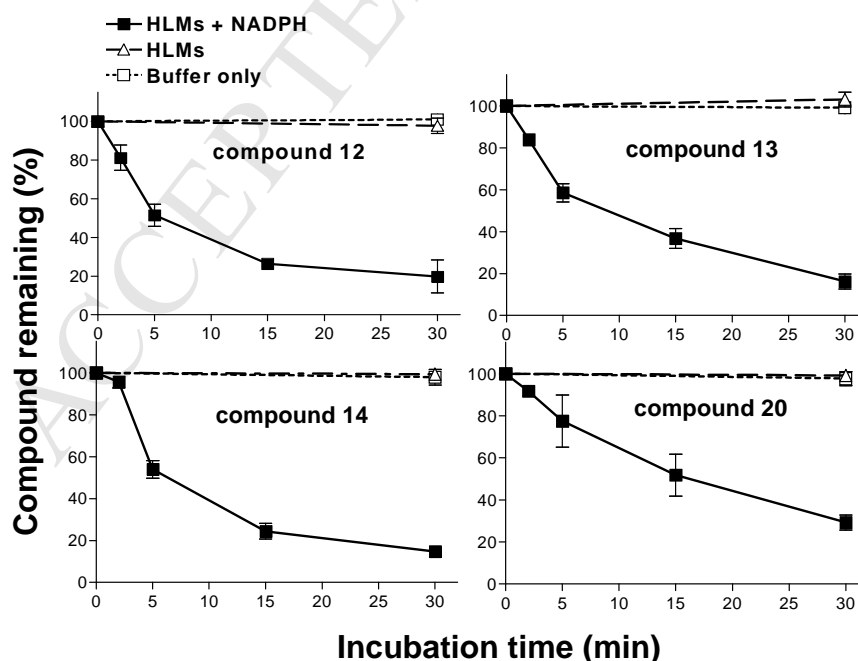


Figure 3. Assessment of metabolic stability of **12**, **13**, **14** and **20** in human liver microsomal incubations. Each compound (10 μ M) was incubated at 37 °C with HLMs (0.5 mg/mL; $-\Delta$ -), HLMs plus 1 mM NADPH ($-\blacksquare$ -), or buffer only (0.1 M KH_2PO_4 , pH 7.4; $-\square$ -). Incubation time points were 0, 2, 5, 15 and 30 min (“HLMs”), or 0 and 30 min (“HLMs plus NADPH” and “buffer only”). The data are expressed as percentage of parent compound remaining at each time compared with time 0 min and represent the mean \pm SD of $n = 3$ independent determinations. Error bars smaller than the symbols are not shown.

Subsequent experiments examined the impact of quercetin, a potent inhibitor of various human drug-metabolizing CYP enzymes, including CYP1A2, CYP2C9, CYP2D6 and CYP3A4 [13-15] on the metabolic stability of compounds **12-14** and **20** in NADPH supplemented-HLMs. As shown in Figure 4, metabolic depletion of all the investigated 7-PPyQ derivatives was significantly inhibited by 100 μ M quercetin. These findings indicate the involvement of one or more human liver microsomal CYPs in the metabolism of compounds **12-14** and **20**.

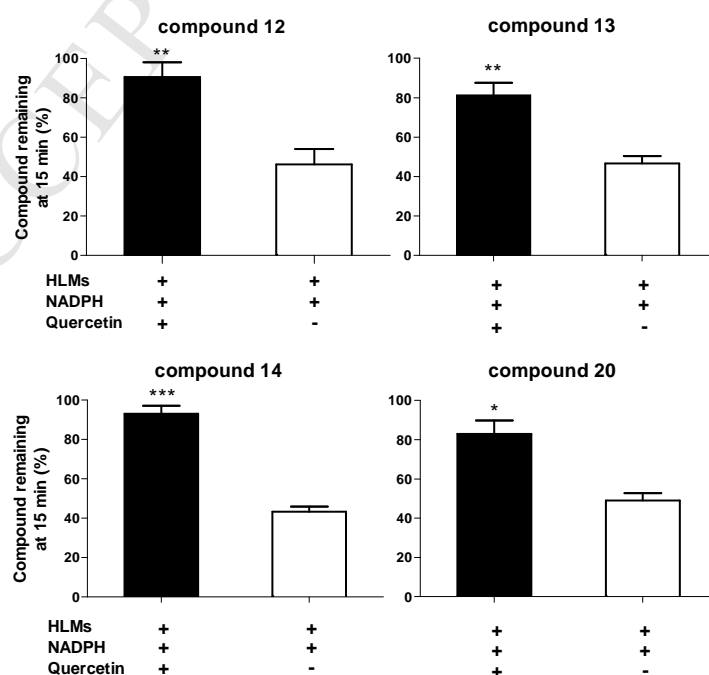


Figure 4. Effect of the CYP inhibitor quercetin on depletion of **12**, **13**, **14** and **20** in NADPH-supplemented human liver microsomal incubations. Each compound (10 μ M) was incubated with HLMs (1 mg/mL) and NADPH (1 mM) at 37 °C for 0 and 15 min, both in the absence and in the presence of 100 μ M quercetin. Each bar represents the percentage (mean \pm SD; n = 3) of compound remaining at 15 min, compared with time 0 min. * P <0.05; ** P <0.01; *** P <0.001

A last set of drug metabolism experiments compared the metabolic stability in HLMs of the monofluorinated 7-PPyQs **15** and **19** with that of their non-fluorinated counterpart 3*N*-benzoyl-7-PPyQ (**21**), an amide compound known to be quite stable to NADPH-dependent metabolism, despite being susceptible to slow hydrolysis catalyzed by HLMs [12]. As shown in Figure 5, for all the tested compounds, a 60-min incubation with HLMs (1 mg of protein/mL) resulted in a modest decline (~ 20%) in the level of compound remaining, regardless of the presence of NADPH in the incubation mixture. Thus, fluorine substitution at the *meta* position of the 7-phenyl ring or the *ortho* position of the benzoyl moiety did not modulate the metabolic stability of compound **21**.

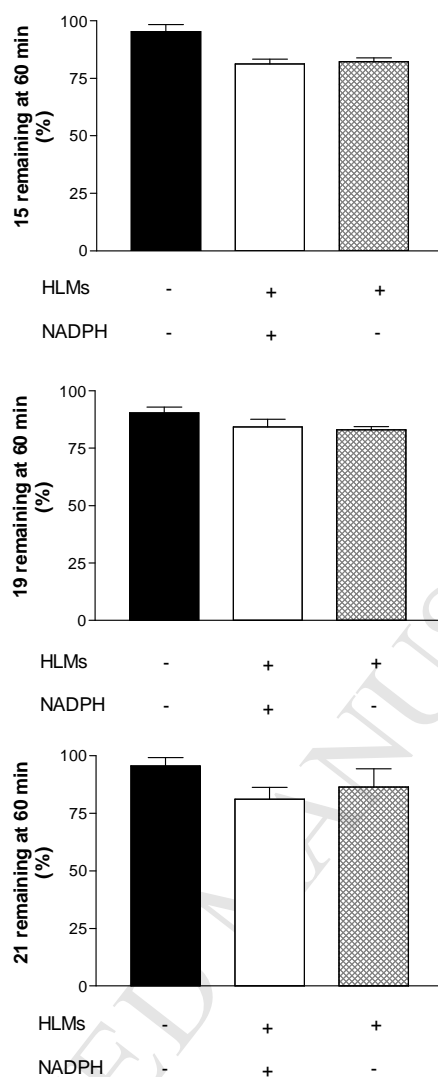


Fig. 5. Assessment of metabolic stability of **15**, **19** and **21** in human liver microsomal incubations. Each compound (10 μ M) was incubated at 37 $^{\circ}$ C with HLMs (1 mg/mL), HLMs plus 1 mM NADPH, or buffer only (0.1 M KH_2PO_4 , pH 7.4) for 0 or 60 min. Each bar represents the percentage (mean \pm SD; n = 3) of compound remaining at 60 min, compared with time 0 min.

2.2.3 *In vitro* antiproliferative activity of compounds **12-15**, **18** and **19**

Evaluation of antiproliferative activities of **12-15**, **18** and **19** was performed with the 3-(4,5-dimethylthiazol-2-yl)-2,5-diphenyltetrazolium bromide (MTT) assay [16] against a panel of 11 human tumor cell lines (DND41, Jurkat, HL-60, RS4;11, MCF-7, MDA-MB-231, MDA-MB-468, HeLa, A375, A2058, HT-29). GI_{50} values, the concentrations that inhibit cell growth

by 50%, are presented in Table 1. From the cytotoxicity data reported in Table 1, we can make some observations on fluoro-derivatives **12-15**, **18** and **19** in comparison with the parent compounds **20** and **21** lacking the fluorine and previously evaluated, as well as on the substitution pattern of the fluorine atom in the 7-PPyQ structure. The *N*-ethyl compounds **12** and **13** have the fluorine atom in the *ortho* and *meta* position, respectively, and they are the most cytotoxic compounds, with nano and sub-nanomolar concentrations. These compounds are comparable with the reference compound **20**. Analog **14**, having the fluorine in the *para* position, is less active with micromolar or high nanomolar GI₅₀s. Between the two *N*-benzoyl compounds **15** and **19**, the derivative **15** with a fluorine in position 3 of the side phenyl is much more cytotoxic than derivative **19** with a fluorine in the *ortho* position of the benzoyl side chain. Finally, among all the fluoro-derivatives, compound **18**, which is unsubstituted at the pyrrolic N and with a fluoro-benzoyl ester in position 9, is the least active. We note that the benzoyl fluoro-derivatives **15** and **19** are less cytotoxic than the reference compound **21**. In conclusion, based on the antiproliferative data shown in Table 1, the preferred substitution sites for a fluorine atom are the *meta* and *ortho* positions of the side phenyl ring, as in compounds **12**, **13** and **15**.

Table 1. *In vitro* cell growth inhibitory effects of compounds **12-15, 18-21**.

Cd	GI ₅₀ ^a (nM)										
	DND-41	Jurkat	HL-60	RS4;11	MCF-7	MDA-MB-231	MDA-MB-468	HeLa	A375	A2058	HT-29
12	0.26±0.088	0.19±0.01	0.17±0.07	0.09±0.005	246.6±12.0	164±43.7	22.3±2.2	1.2±0.1	15.5±1.5	4.8±0.2	1.1±0.2
13	0.13±0.020	0.11±0.02	0.08±0.002	0.07±0.006	52.7±10.7	69±6.0	15.0±1.1	0.7±0.05	11.4±2.0	3.5±0.4	0.9±0.1
14	476.7±128.1	333.5±12.1	1440±42.4	293.3±61.7	51.3±9.9	206±8.3	43.0±12.6	340±18.4	69.8±5.9	1180±90.7	447±12.0
15	10.2±0.160	32.4±2.2	15.1±0.090	56±12	103±50	454±48	871±60	13.3±0.9	n.d.	n.d.	402±37
18	2425±425	323.5±29.1	2307±77	696.7±72.6	3464±231.5	5591±500.4	1318±68.4	501±34.4	2553±139.6	1493±127	216±17.1
19	240.0±15.3	53.7±20.2	276.0±20.9	119.7±25.4	1082±24.9	3031±340.4	70±15.7	9.3±1.1	332±13.6	322±12.5	26.6±2.0
20	nd	0.5±0.2	0.5±0.02	2±0.3	40±10	nd	nd	11±8	nd	Nd	32±1.2
21	nd	16±0.6	2±0.8	0.3±0.0001	0.2±0.0.1	nd	nd	0.2±0.0.4	nd	Nd	0.1±0.1

^aGI₅₀= compound concentration required to inhibit tumor cell proliferation by 50%. Data are presented as the mean ± SE from the dose-response curves of at least three independent experiments. N.d. not determined.

2.2.4 Evaluation of cytotoxicity of compounds **12**, **13**, **15**, **20** and **21** in human non-cancer cells

To obtain a preliminary indication of the cytotoxic potential of these derivatives in normal human cells, three of the most active compounds (**12**, **13** and **15**) along with compounds **20** and **21** chosen for comparison as non-fluorinated compounds, were evaluated *in vitro* against peripheral blood lymphocytes (PBL) from healthy donors (Table 2). All compounds showed very low activity in quiescent lymphocytes ($GI_{50} > 10 \mu\text{M}$), while in the presence of the mitogenic stimulus phytohematoagglutinin (PHA), the GI_{50} values were slightly decreased but remained in the higher micromolar range. These values were almost 10000-30000 times higher than those observed against the lymphoblastic cell lines Jurkat, DND-41 and CEM (Tables 1 and 3). Thus, these compounds have only a modest inhibitory effect in primary lymphocytes, as previously observed for other antimitotic derivatives developed by our group [10].

Table 2. Cytotoxicity of compounds **12**, **13**, **15**, **20** and **21** for human peripheral blood lymphocytes (PBL)

Cd	GI_{50} (μM) ^a	
	PBL _{resting} ^b	PBL _{PHA} ^c
12	28.0±2.3	15.2±6.9
13	31.3±10.3	10.8±3.8
15	45.6±6.3	17.6±3.9
20	>100	7.6±0.06
21	>100	2.7±1.3

^a Compound concentration required to inhibit cell growth by 50%. Values are the mean ± SEM for three separate experiments

^b PBL not stimulated with PHA.

^c PBL stimulated with PHA.

2.2.5 Effect of compounds **12**, **13**, **15**, **20** and **21** on multidrug resistant cells

To investigate whether these derivatives are substrates of drug efflux pumps, compounds **12**, **13** and **15** were tested against the CEM^{Vbl-100} cell line that is a multidrug-resistant line selected against vinblastine [17] and that overexpress P-glycoprotein (P-gp). This membrane protein acts as a drug efflux pump and exhibits resistance to a wide variety of structurally unrelated anticancer drugs and other compounds. As shown in Table 3, all the compounds exhibited cytotoxic activity in the CEM^{Vbl100} cell line that was even higher than their activity against the parental line, indicating that these derivatives are not substrates for P-gp.

Table 3. Cytotoxicity of **12**, **13**, **15**, **20** and **21** in multidrug resistant cell lines

Cd	GI ₅₀ (nM) ^a	
	CEM ^{wt}	CEM ^{V61100}
12	3.1±0.2	1.1±0.4
13	2.2±0.3	0.8±0.3
15	44±6	36±10
20	14.0±0.4	4.0±0.4
21	2.5±0.6	3.1±0.4

^a Compound concentration required to reduce cell growth by 50%. Values are the mean ± SEM for three separate experiments.

2.2.6 Inhibition of tubulin polymerization and colchicine binding

To evaluate the antitubulin properties of the new compounds, we investigated their effects on the inhibition of tubulin polymerization and on the binding of [³H]colchicine to tubulin (Table 4) [18, 19]. For comparison, CSA-4 was examined in contemporaneous experiments as a reference compound. Among the test compounds, **12**, **13** and **15** strongly inhibited tubulin assembly with IC₅₀ values below 1 μM (0.96, 0.84 and 0.38 μM, respectively), with **12** and **13** slightly less active than CSA-4 (IC₅₀=0.64 μM) and compound **15** more active than CSA-4. These results with tubulin correlate well with the growth inhibitory effects exhibited by these compounds, indicating that their antiproliferative activity derives from an interaction with tubulin. The other compounds also inhibited tubulin assembly, with IC₅₀ values in the range of 1.3-3.7 μM. All compounds inhibited the binding of [³H]colchicine to tubulin, with the best

activity occurring with **12**, **13** and **15**, but none approached CSA-4 in its potency as an inhibitor of colchicine binding.

Table 4. Inhibition of tubulin polymerization and colchicine binding by compounds **12-15** and **19-21**

Cd	Inhibition of tubulin assembly IC ₅₀ (μM) ± SD ^a	Inhibition of colchicine binding % Inhibition ± SD ^b
12	0.96±0.08	77±3
13	0.78±0.03	83±5
14	3.7± 0.4	12±4
15	0.38±0.03	70±0.8
19	1.3±0.07	34±4
CSA-4	0.64±0.1	100±2
20^c	0.57±0.02	73±0.7
21^d	0.89±0.04	70±0.20
CSA-4^{c, d}	1.2±0.1	98±0.7

a Inhibition of tubulin polymerization. Tubulin was at 10 μM.

b Inhibition of [³H]colchicine binding. Tubulin and colchicine were at 1 and 5 μM concentrations, respectively.

c Data taken from reference [10]

d Data taken from reference [11]

2.2.7 Influence of test compound **12** on the cell cycle

The effect of compound **12**, taken as representative of a fluoro-PPyQ derivative, on cell cycle progression was examined by flow cytometry in two melanoma cell lines (A375 and A2380). After a 24 h treatment, **12**, evaluated at the concentrations of 50 and 100 nM, induced a strong G2/M arrest at both concentrations in both cell lines (Figure 6, Panels A and B). A concomitant reduction of both the S and G1 phases was also observed. In order to determine whether **12** was able to block cells at the mitotic phase (M), cells were stained with an immunofluorescent antibody to p-histone H3, a well-known mitotic marker [20], as well as PI, and analyzed by flow cytometry. As shown in Figure 6 (Panel C), HeLa cells arrested in M phase by treatment with **12** are readily distinguished from G2 cells by the higher level of p-histone H3. In particular, treatment with **12** induced an increase in the percentage of mitotic cells from 1.5% observed in untreated cells to about 10% and 44 % with 50 and 100 nM concentrations, respectively. We also studied the association between **12**-induced G2/M arrest and alterations in G2/M regulatory protein expression in HeLa cells. As shown in Figure 7 compound **12** caused an increase in cyclin B1 expression after 24 and 48 h in a concentration-dependent manner, indicating an activation of the mitotic checkpoint following drug exposure.

This effect was confirmed by a reduction in the expression of phosphatase cdc25c at 24 h, followed by a disappearance in its expression at 48 h. This was associated with the appearance of slower migrating forms of phosphatase cdc25c indicating its phosphorylation. The phosphorylation of cdc25c directly stimulates its phosphatase activity, and this is necessary to activate cdc2/cyclin B on entry into mitosis [21, 22]. We also observed a decrease of the phosphorylated form of cdc2 kinase, in particular after the 48 h treatment.

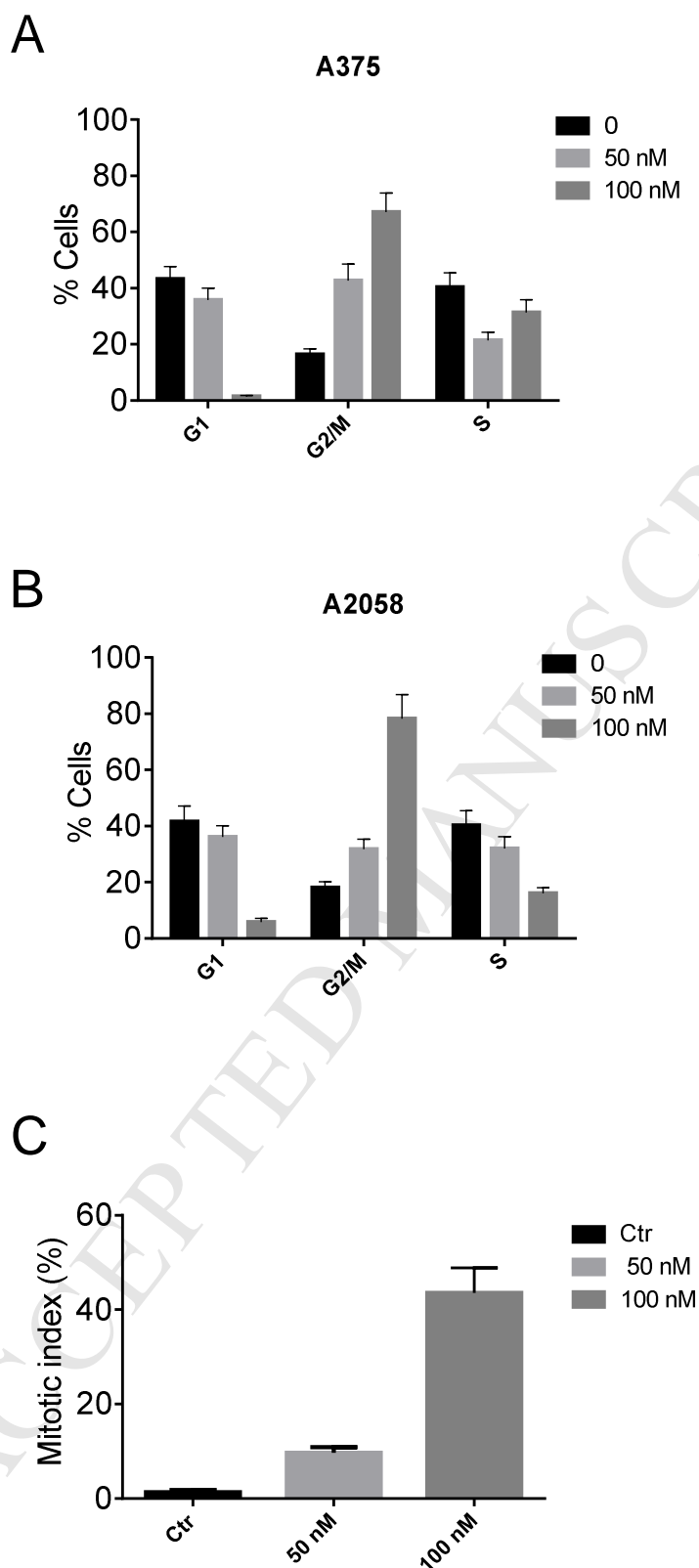


Figure 6. Percentage of cells in each phase of the cell cycle in A375 (Panel A) and A2058 (Panel B) cells treated with compound **12** at the indicated concentrations for 24 h. Cells were fixed and labeled with PI and analyzed by flow cytometry as described in the Experimental

Section. Data are represented as mean of two independent experiments \pm SEM. Panel C. Mitotic index evaluated in HeLa cells with compound **12** after a 24 h treatment with **12** at the indicated concentrations.

2.2.8 Compound **12** induces apoptosis in HeLa cells

To evaluate the mode of cell death induced by test compounds, we performed a bi-parametric cytofluorimetric analysis using propidium iodide (PI) and annexin-V-FITC, which stain DNA and phosphatidylserine (PS) residues, respectively [23, 24]. We used HeLa cells to evaluate these effects of compound **12**. As shown in Figure 8, the compound induced apoptosis in a time and concentration dependent manner, even at the lower concentration used (50 nM).

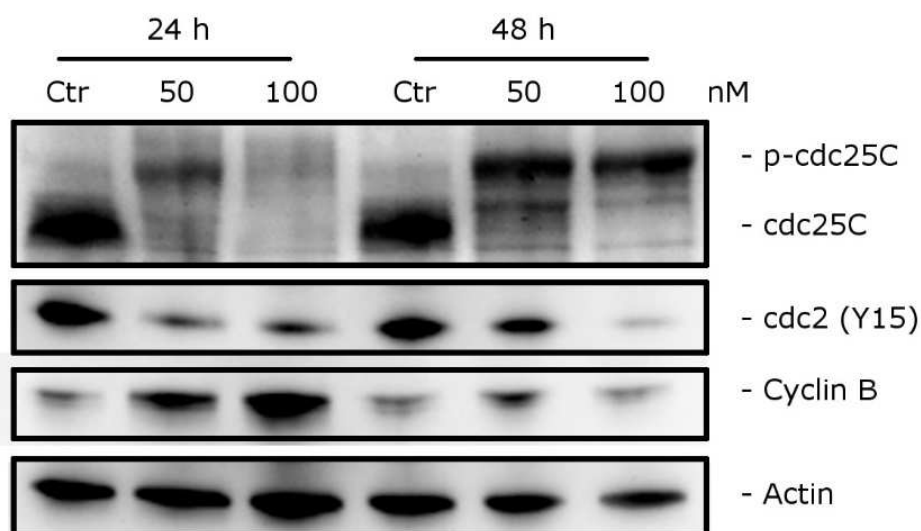
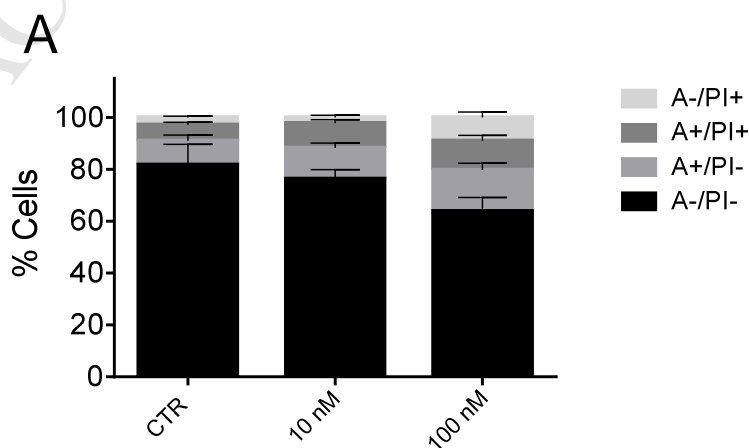


Figure 7. Effect of compound **12** on cell cycle checkpoint proteins. HeLa cells were treated for 24 or 48 h with the indicated concentrations of **12**. The cells were harvested and lysed for detection of the expression of the indicated protein by western blot analysis. To confirm equal protein loading, each membrane was stripped and reprobbed with anti- γ -actin antibody.

2.2.9 Compound **12** induced mitochondrial depolarization and reactive oxygen species (ROS) production

Mitochondria play an essential role in the propagation of apoptosis [25, 26]. It is well established that, at an early stage, apoptotic stimuli alter the mitochondrial transmembrane potential ($\Delta\psi_{mt}$). $\Delta\psi_{mt}$ was monitored by the fluorescence of the dye JC-1 [27]. HeLa cells treated with compound **12** (10-100 nM) showed a time-dependent increase in the percentage of cells with low $\Delta\psi_{mt}$ (Figure 9, Panel A). The depolarization of the mitochondrial membrane is associated with the appearance of annexin-V positivity in the treated cells when they are in an early apoptotic stage. In fact, the dissipation of $\Delta\psi_{mt}$ is characteristic of apoptosis and has been observed with both microtubule stabilizing and destabilizing agents, including other 7-PPyQ derivatives, in different cell types [28-31]. It is well known that mitochondrial membrane depolarization is associated with mitochondrial production of ROS [32, 33]. Therefore, we investigated whether ROS production increased after treatment with the test compounds. We utilized the fluorescence indicator 2,7-dichlorodihydrofluorescein diacetate (H_2 -DCFDA)[33]. As shown in Figure 9 (Panel B) compound **12** induced significant production of ROS starting after 12-24 h of treatment at 100 nM, in good agreement with the mitochondrial depolarization described above.



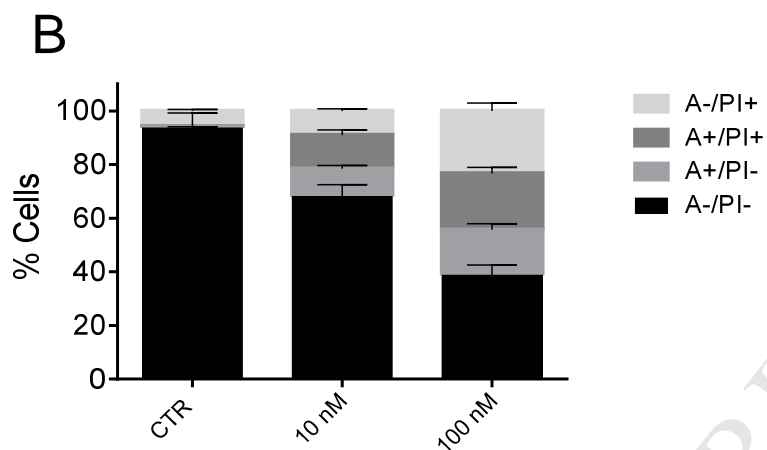


Figure 8. Flow cytometric analysis of apoptotic cells after treatment of HeLa (Panels A and B) cells with compound **12** at the indicated concentrations after incubation for 24 (A) or 48 h (B). The cells were harvested and labeled with annexin-V-FITC and PI and analyzed by flow cytometry. Dual staining for annexin-V and with PI permits discrimination between live cells (annexin-V⁻/PI⁻), early apoptotic cells (annexin-V⁺/PI⁻), late apoptotic cells (annexin-V⁺/PI⁺) and necrotic cells (annexin-V⁻/PI⁺). Data are represented as mean±SEM of three independent experiments.

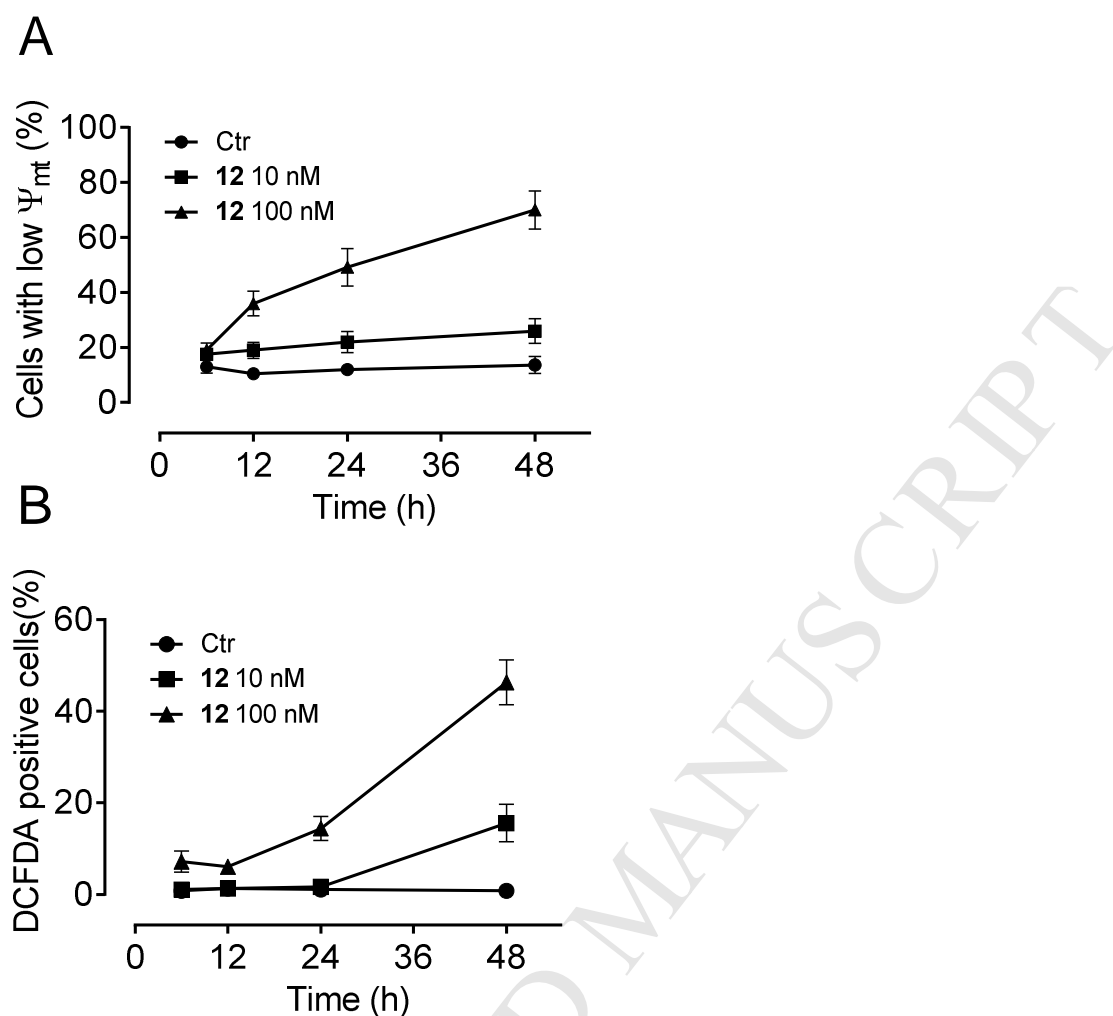


Figure 9. Panel A. Assessment of mitochondrial membrane potential ($\Delta\Psi_{mt}$) after treatment of HeLa cells with compound **12**. Cells were treated with the indicated concentrations of compound for 6, 12, 24 and 48 h and then stained with the fluorescent probe JC-1 for analysis of mitochondrial potential. Cells were then analyzed by flow cytometry as described in the experimental section. Data are presented as mean \pm SEM of three independent experiments. Panel B. Assessment of ROS production after treatment of HeLa cells with compound **12**. Cells were treated with the indicated concentrations of compound for 6, 12, 24, and 48 h and then stained with H₂-DCFDA for the evaluation of ROS levels. Cells were then analyzed by flow cytometry as described in the experimental section. Data are represented as mean \pm SEM of three independent experiments.

2.2.10 Compound 12 induced caspase-3 and poly (ADP-Ribose) polymerase (PARP) activation and caused a decrease in the expression of anti-apoptotic proteins

As shown in Figure 10, compound **12** in HeLa cells caused a concentration and time-dependent increase of the cleaved fragment of caspase-3 and concomitantly the cleavage of PARP, confirming its pro-apoptotic activity.

We also investigated the expression of anti-apoptotic proteins, such as Bcl-2 and Mcl-1. Bcl-2 plays a major role in controlling apoptosis through the regulation of mitochondrial processes and the release of mitochondrial proapoptotic molecules that are important for the cell death pathway [35-37]. Our results (Figure 10) showed that the expression of the anti-apoptotic protein Bcl-2 was decreased starting after a 24 h treatment at both concentrations of **12** used (10 and 100 nM). The decrease in expression of Mcl-1 was even greater.

Interestingly, as observed for other antimetabolites, we observed after treatment with **12** a significant increase in the expression of the phosphohistone H2AX, a well-known marker of DNA damage. In this context, it is worthwhile noting that prolonged mitotic arrest may induce DNA damage that ultimately leads to apoptosis.

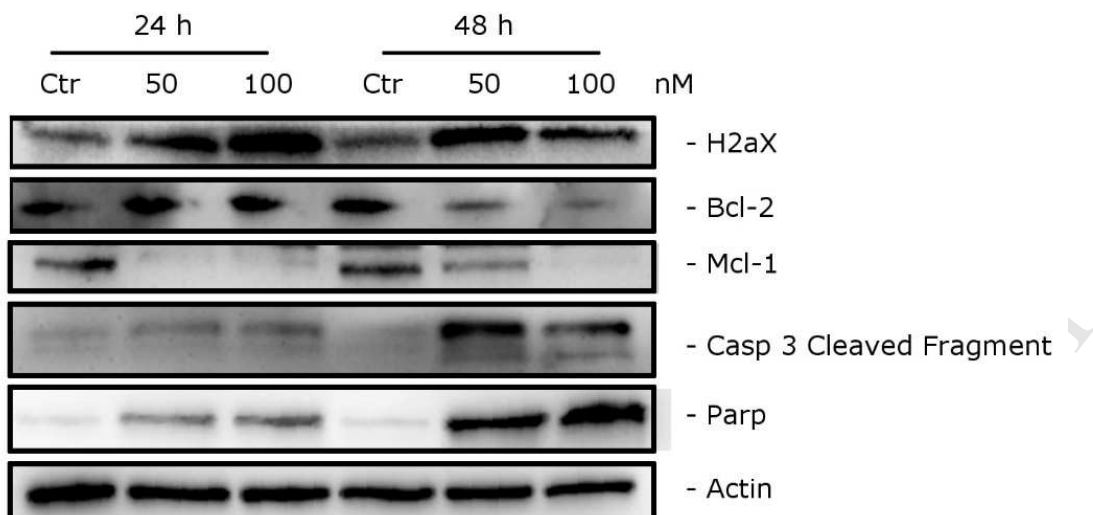


Figure 10. Western blot analysis of Bcl-2, Mcl-1 and PARP after treatment of HeLa cells with **12** at the indicated concentrations and for the indicated times. To confirm equal protein loading, each membrane was stripped and reprobbed with anti- γ -actin antibody.

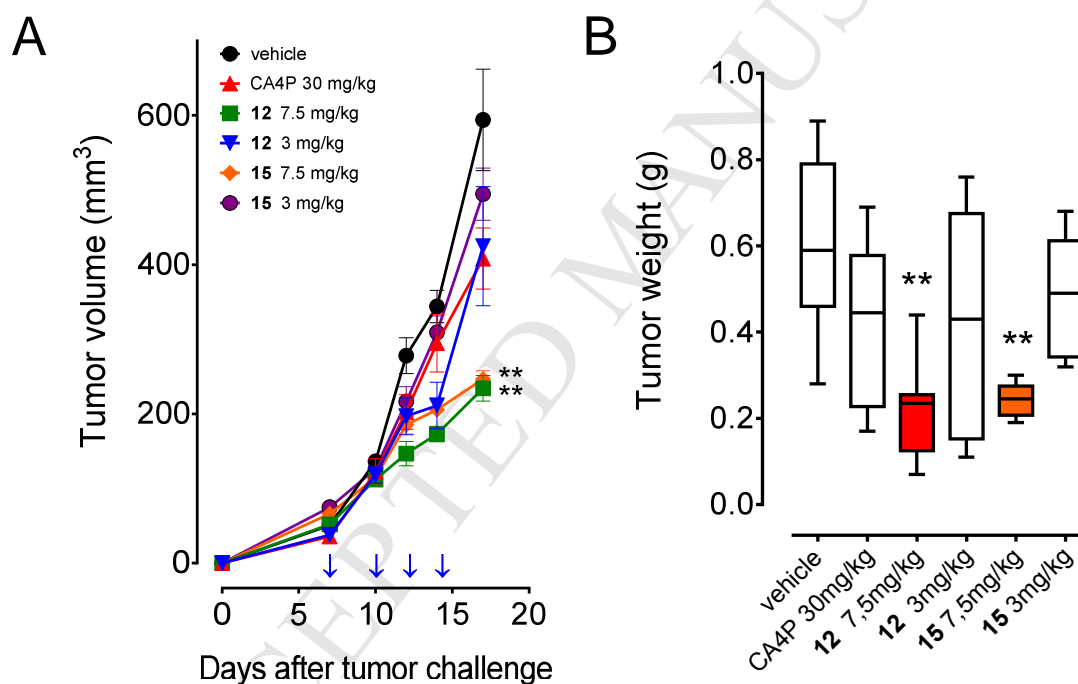
2.2.11 Evaluation of the antitumor activity of compounds **12** and **15** *in vivo*.

To determine the *in vivo* antitumor activity of **12** and **15**, a syngeneic murine model was used [38], the BL6-B16 mouse melanoma cell line. Preliminary *in vitro* experiments were carried out to evaluate the cytotoxicity of these compounds in this cell line. The GI_{50} obtained after 72 h was 10 ± 4 nM and 18 ± 6 nM, for **12** and **15**, respectively.

BL6-B16 cells were injected subcutaneously in syngeneic C57BL/6 mice. Once the tumor reached a measurable size (about 100 mm^3), mice were randomly assigned to different experimental groups and treated intraperitoneally every other day with vehicle (DMSO) or one of the two compounds (at doses of 7.5 or 3.0 mg/kg) or with combretastatin A4 phosphate (CA4P) ((at 30 mg/kg) as a reference compound.

As shown in Figure 11 (Panel A), both compounds **12** and **15** caused a similar and significant reduction in the growth of BL6-B16 melanoma cells at the dose of 7.5 mg/kg (60% for **12** and

58.4% for **15**) in comparison with the vehicle-treated group. Also, at the dose of 3 mg/kg we observed a significant reduction of the tumor mass only for compound **12** (28.6%), whereas the result with compound **15** did not reach statistical significance (16.7%). Notably, treatment with the reference compound CA4P at 30 mg/kg caused only a small reduction in tumor volume (31.3 %) if compared with both doses of compound **12**. From the safety/tolerability point of view, no significant variation in body weight occurred in animals treated with either **12** and **15** at the higher concentration (Figure 11, panel C).



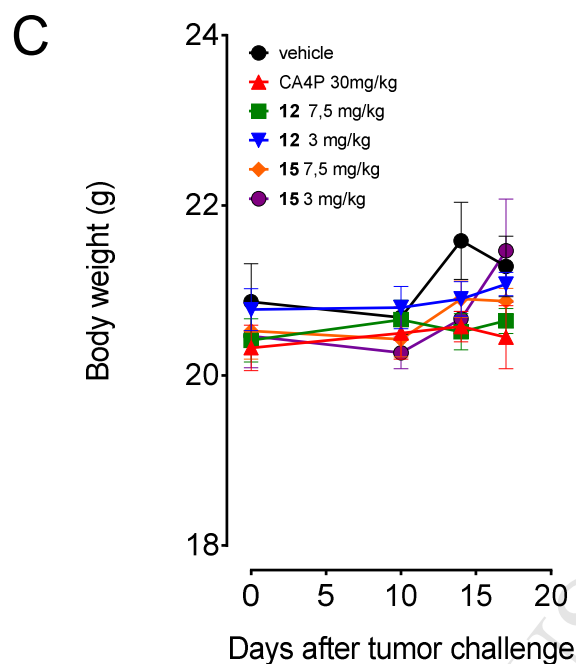


Figure 11. Inhibition of mouse allograft growth *in vivo* by compounds **12** and **15**. Panel A: male C57BL/6 mice were injected subcutaneously at their dorsal region with 10^7 BL6-B16 murine melanoma cells. Tumor-bearing mice were administered the vehicle, as control, or 7.5 and 3.0 mg/kg of **12** and **15** or CA4P as reference compound at 30 mg/kg. Injections were given intraperitoneally on the days indicated by the arrows. Panel B: tumor weight registered at the end of the treatment. Panel C: body weight variation after treatment with **CA-4P**, **12** and **15**. Data are presented as mean \pm SEM of tumor volume at each time point for 5 animals per group. $**p < 0.01$ vs. control.

2.3 Molecular modelling

Molecular docking studies were carried out to investigate the possible binding mode of the synthesized compounds with the aim of interpreting the biological data. Recently, we reported a study to identify the best docking protocol and the protein conformation most suitable to accommodate the 7-PPyQ scaffold [11]. Taking advantage of our previous findings, we docked derivatives: **12-15**, **18** and **19**. According with the previously reported 7-PPyQ

derivatives, the most potent compounds occupy the colchicine site and establish a key hydrogen bond mediated by the 7-PPyQ scaffold with the polypeptide backbone with β Val236. In addition, the fused-ring system guarantees strong hydrophobic interactions with β Leu253, β Ala314, and β Ile368, while the aromatic substituents at position 7 establish hydrophobic interactions with residues β Phe167, β Tyr200, and β Leu250. The substituents at the *N*-pyrrole are accommodated in the pocket formed by residues β Lys350, β Thr351, β Ala314, β Ala352, and β Thr179. The introduction of the fluorine atom on the phenyl ring at position 7 seems not to affect the orientation of the ring; compounds **12**, **13** and **14**, respectively fluorinated at the *ortho*, *meta* and *para* position, present the same orientation as the reference compound **21** (Figure 1), in which the phenyl ring and the PyQ fused system are reciprocally orthogonal. Interestingly, when the fluorine atom is at the *ortho* or *meta* position, it is preferentially faced toward two distinct pocket regions: for compound **13** and **15** (*meta*) the fluorine points to residues β Asn165- β Phe167, while in **12** (*ortho*) it is oriented towards β Cys299 and β Leu240. Also, in the case of fluorination of the phenyl ring at the *N*-pyrrole 3 (compound **19**), the binding mode is unchanged, and the fluorine atom faces toward β Thr179.

To further evaluate the geometric and energetic stability of these binding modes, all the docked conformations were subjected to three different MD simulations at the length of 10 ns each, and the RMSD as well as the MMGBSA were computed. As a reference, the non-fluorinated compound **21** was included in similar calculations. The ligands **12-15**, **19** and **21** showed notable stability with a RMSD below 1 Å (Table SI 1). In addition, MMGBSA values also confirm the stability of the complexes, with values from -40.1 to -48.1 kcal/mol.

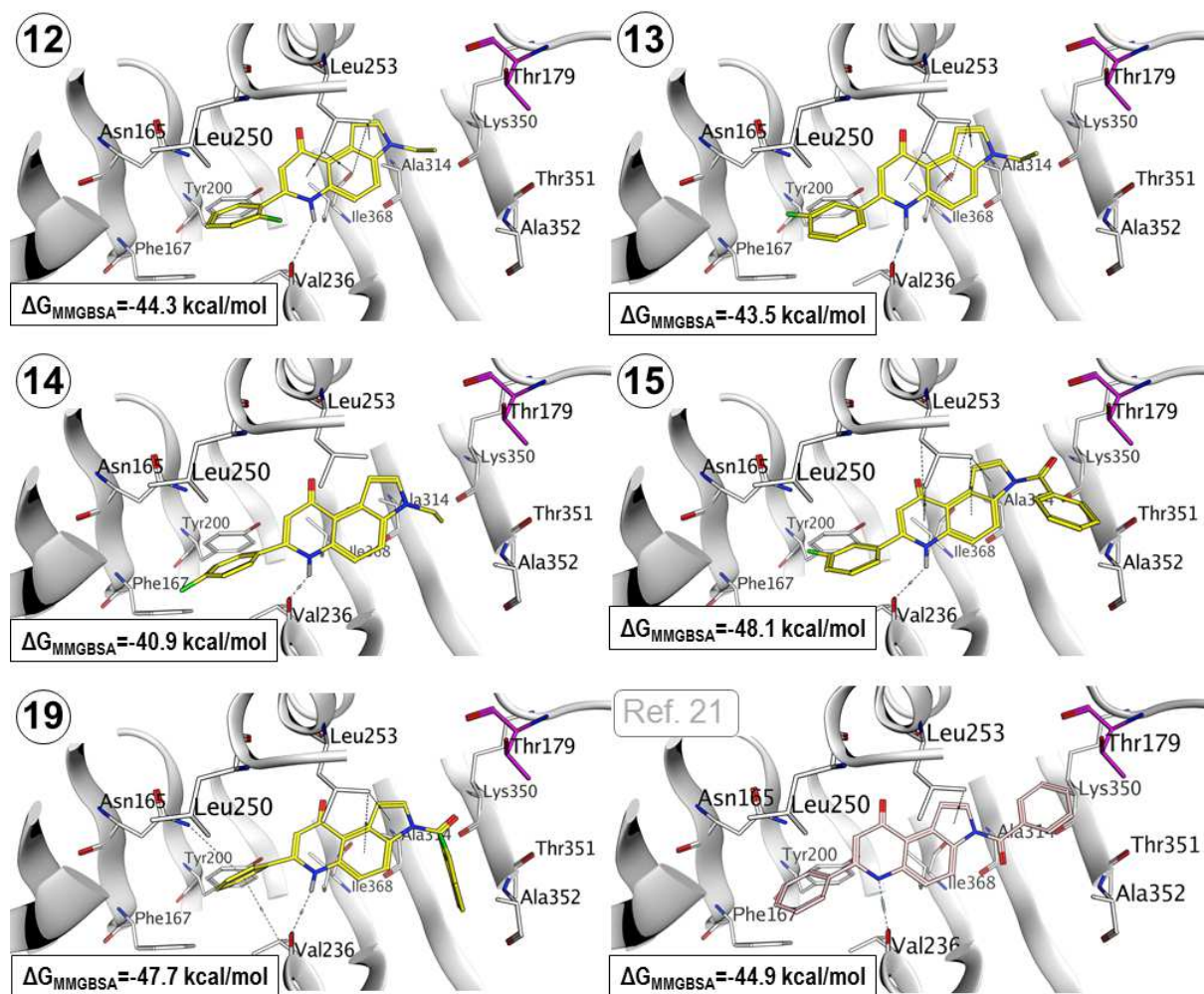


Figure 12. The energetically most favorable poses for all the compounds in Table 1. Molecular docking simulations using the protein conformation of the plinabulin complex (PDB ID: 5C8Y), with the carbon atoms of the synthesized compounds colored in yellow. The reference non-fluorinated compound **21** is rendered using pink for the carbon atoms. The residue atoms of the colchicine site are colored according to the subunit to which they belong: white for β -tubulin and magenta for α -tubulin. Hydrogen atoms are not shown.

3. Conclusions

The monofluoro 7-PPyQ derivatives **12-14**, and **19** were designed to improve the metabolic stability of the known parent compounds **20** and **21**. To obtain more information on the possible impact of fluorination on the biological properties of this class of compounds, our library was completed with the monofluoro 7-PPyQs **15** and **18**. Since fluorination might influence both therapeutic efficacy and target affinity [5], we evaluated the cytotoxicity of the newly synthesized compounds against various human tumor cell lines and their activities with tubulin (inhibition of assembly and of colchicine binding to tubulin).

The fluorinated 7-PPyQ derivatives **12-15** and **19** retained high cytotoxicity, with compounds **12**, **13** and **15** at least as active as the parent compounds (GI_{50} values in the nano- or sub-nanomolar range). The molecular target was confirmed, since most of the newly prepared compounds strongly inhibited tubulin polymerization, with **15** more inhibitory than the reference compound CSA-4 (IC_{50} s of 0.38 and 0.64 μ M, respectively), but CSA-4 was more potent than **15** as an inhibitor of colchicine binding. The 4-fluoro-phenyl derivative **14** was less potent than its isomeric 2- and 3-fluoro derivatives **12** and **13** in inhibiting tubulin assembly, and this data correlated with its lower *in vitro* cytotoxic activity (Table 1). Our docking studies suggested that the effect induced by the electron-rich fluorine in the 2-position of **14** is unfavorable for optimal binding in the colchicine site as compared with the other two monofluoro analogues. *In vitro* experiments also showed that **12**, **13** and **15** have only modest cytotoxic effects on primary lymphocytes, as previously observed for other antimitotic derivatives developed by our group [8-11]. This class of compounds is also active against the P-gp-expressing CEM^{Vb1100} cell line.

Compound **12**, chosen as a representative of the fluoro-PPyQs, induced a strong G2/M cell cycle arrest in two human melanoma cell lines. In HeLa cells, compound **12** caused mitotic arrest and induced apoptosis in a time- and concentration-dependent manner, and triggered mitochondrial depolarization with significant production of ROS.

In accord with the cytotoxicity data summarized in Table 1, molecular docking studies suggested that the presence of a fluorine atom in different positions of the 7-PPyQ system does not significantly affect the binding mode of **12-15** and **19** into the colchicine site of tubulin. Furthermore, our results indicate the substitution of fluorine in place of hydrogen in the *ortho*, *meta* or *para* position of the 7-phenyl ring of compound **20** or in the 2-position of the benzoyl moiety of **21**, did not lead to compounds with improved metabolic stability. Finally, the *in vivo* data showing that both **12** and **15** were effective in significantly slowing the growth of tumors derived from BL6-B16 melanoma cells are quite promising and suggest that these fluorinated 7-PPyQs deserve further investigation as potential anti-cancer drugs.

4. Experimental section

4.1 Chemistry

Melting points were determined on a Buchi M-560 capillary melting point apparatus and are uncorrected. ^1H and ^{13}C NMR spectra were determined on Bruker 300 and 400 MHz spectrometers, with the solvents indicated; chemical shifts are reported in δ (ppm) downfield from tetramethylsilane as internal reference. Coupling constants are given in hertz. In the case of multiplets, chemical shifts were measured starting from the approximate centre. Integrals were satisfactorily in line with those expected based on compound structure. Mass spectra were obtained on a Mat 112 Varian Mat Bremen (70 eV) mass spectrometer and Applied Biosystems Mariner System 5220 LC/MS (nozzle potential 140 eV). Column flash chromatography was performed on Merck silica gel (250–400 mesh ASTM); chemical reactions were monitored by analytical thin-layer chromatography (TLC) on Merck silica gel 60 F-254 glass plates. Microwave assisted reactions were performed on a CEM Discover® monomode reactor with a built-in infrared sensor assisted-temperature monitoring and automatic power control; all reactions were performed in closed devices under pressure

control. Solutions were concentrated on a rotary evaporator under reduced pressure. The purity of new tested compounds was checked by HPLC using the instrument HPLC VARIAN ProStar model 210, with detector DAD VARIAN ProStar 335. The analysis was performed with a flow of 1 mL/min, a C-18 column of dimensions 250 mm X 4.6 mm, a particle size of 5 μ m, and a loop of 10 mL. The detector was set at 300 nm. The mobile phase consisted of phase A (Milli-Q H₂O, 18.0 MU, TFA 0.05%) and phase B (95% MeCN, 5% phase A). Gradient elution was performed as follows: 0 min, % B = 10; 0 and 20 min, % B = 90; 25 min, % ; B = 90; 26 min, % B = 10; 31 min, % B = 10.

Starting materials were purchased from Sigma-Aldrich and Alfa Aesar, and solvents were from Carlo Erba, Fluka and Lab-Scan. DMSO was made anhydrous by distillation under vacuum and stored on molecular sieves.

4.1.1 1-Ethyl-5-nitro-1H-indole (**1**).

Into a two-necked 100 mL round-bottomed flask, 0.666 g (27.75 mmol) of NaH, 60% dispersion in mineral oil, was placed and washed with toluene (3 \times 10 mL). With stirring, a solution of commercial 5-nitroindole, 1.500 g (9.25 mmol) in 5 mL of anhydrous DMF was dropped into the flask, and the initial yellow color changed to red with the formation of H₂ gas. After 40 min at room temperature, the mixture was cooled to 0 °C, and 2.00 mL (26.61 mmol, d=1.46 g/mL) of bromoethane was dropped into the flask, followed by 0.050 g of NaI. The reaction was monitored by TLC analysis (eluent toluene/*n*-hexane/ethyl acetate, 1:1:1). At the end of the reaction, 25 mL of water was added, and the solvent was evaporated under reduced pressure, leaving a residue, which was extracted with ethyl acetate (3 \times 30 mL). The organic phase, washed with water, brine, and dried over anhydrous Na₂SO₄, was concentrated under vacuum giving 1.69 g of a yellow solid. Yield: 99%; R_f: 0.63 (toluene/*n*-hexane/ethyl acetate, 1:1:1); mp = 94 °C; ¹H NMR (300 MHz, DMSO-d₆): δ 7.74 (d, J = 2.1 Hz, 1H, H-4),

7.20 (dd, $J = 9.0, 2.1$ Hz, 1H, H-6), 6.87 (m, 2H, H-7 e H-3), 5.93 (d, $J = 3.3$ Hz, 1H, H-2), 3.47 (q, $J = 7.1$ Hz, 2H, CH₂), 0.55 (t, $J = 7.1$ Hz, 3H, CH₃), ppm; HRMS (ESI-MS, 140 eV): m/z [M+H]⁺ calculated for C₁₀H₁₁N₂O₂⁺, 191.2035; found, 191.1859.

4.1.2 (5-Nitro-1H-indol-1-yl)(phenyl)methanone (2).

Into a 50 mL round-bottomed flask, a solution of 5-nitroindole 0.500 g (3.08 mmol, 1 eq.) in 20 mL of CH₂Cl₂ was treated with DMAP (0.692 g, 6.17 mmol, 2 eq.) and pyridine (0.500 mL, 6.17 mmol, 2 eq.). The mixture was cooled to 0 °C, and a solution of benzoyl chloride in CH₂Cl₂ (0.716 mL, 6.17 mmol, 2 eq.) was dropped into the flask. The reaction mixture was stirred at room temperature for 24 h. The reaction was monitored by TLC analysis (eluent CH₂Cl₂/petroleum ether/EtOAc, 3:6,5:0,5). At the end, the reaction was quenched by adding a solution of HCl 0.5 M, and the aqueous phase was extracted with CH₂Cl₂ (3 x 50 mL). The combined organic extracts were dried over MgSO₄, concentrated under vacuum, dissolved in a mixture of CH₂Cl₂/petroleum ether/EtOAc, 3:6.5:0.5 and filtered through SiO₂ giving a pale-yellow solid (0.443 g, 1.67 mmol, 54%). Yield = 54%; R_f: 0.61 (eluent CH₂Cl₂/petroleum ether/EtOAc, 3:6,5:0,5); mp = 312 °C; ¹H NMR (300 MHz, CDCl₃) δ 8.53 (d, $J = 2.2$ Hz, 1H, H-4), 8.49 (d, $J = 9.1$ Hz, 1H, H-7), 8.27 (dd, $J = 9.1, 2.3$ Hz, 1H, H-6), 7.80 – 7.73 (m, 2H, H-2' and H-6'), 7.67 (ddd, $J = 6.6, 3.9, 1.4$ Hz, 1H, H-4'), 7.57 (ddd, $J = 6.6, 4.5, 1.3$ Hz, 2H, H-3' and H-5'), 7.50 (d, $J = 3.8$ Hz, 1H, H-2), 6.77 (dd, $J = 3.8, 0.5$ Hz, 1H, H-3) ppm; HRMS (ESI-MS, 140 eV): m/z [M+H]⁺ calculated for C₁₅H₁₁N₂O₃⁺, 267.0764; found, 267.0745.

4.1.3 (2-fluorophenyl)(5-nitro-1H-indol-1-yl)methanone (3).

Into a 50 mL round-bottomed flask, a solution of 5-nitroindole 0.500 g (3.08 mmol, 1 eq.) in 20 mL of CH₂Cl₂ was treated with DMAP (0.692 g, 6.17 mmol, 2 eq.) and pyridine (0.500

mL, 6.17 mmol, 2 eq.). The mixture was cooled to 0 °C, and a solution of 2-fluoro-benzoyl chloride (**17**) in CH₂Cl₂ (0.978 g, 6.17 mmol, 2 eq.) was dropped into the flask. The reaction mixture was stirred at room temperature for 24 h. The reaction was monitored by TLC analysis (eluent CH₂Cl₂/petroleum ether/EtOAc, 3:6.5:0.5). At the end, the reaction was quenched by adding a solution of HCl 0.5 M and the aqueous phase was extracted with CH₂Cl₂ (3 x 50 mL). The combined organic extracts were dried over MgSO₄, concentrated under vacuum, dissolved in a mixture of CH₂Cl₂/petroleum ether/EtOAc, 3:6.5:0.5 and filtered through SiO₂ giving a yellow solid (0.543 g, 1.90 mmol, 62%). Yield = 62%; R_f: 0.61 (eluent CH₂Cl₂/petroleum ether/EtOAc, 3:6.5:0.5); mp = 326 °C ; ¹H NMR (300 MHz, CDCl₃) δ 8.71 (dd, *J* = 2.0, 1.9 Hz, 1H), 8.24 (dd, *J* = 8.8, 1.9 Hz, 1H), 7.99 (m, *J* = 8.8, 0.5 Hz, 1H), 7.82 (m, *J* = 8.7 Hz, 1H), 7.73 (m, *J* = 8.1, 1.5 Hz, 1H), 7.51 (m, *J* = 8.3, 7.4 Hz, 1H), 7.44 (m, *J* = 8.3, 1.3 Hz, 1H), 7.32 (dd, *J* = 8.1, 7.4 Hz, 1H), 6.88 (m, *J* = 8.7, 2.0 Hz, 1H) ppm; HRMS (ESI-MS, 140 eV): *m/z* [M+H]⁺ calculated for C₁₅H₁₀FN₂O₃⁺, 285.0670; found, 285.0618.

4.1.4 1-Ethyl-1H-indol-5-amine (**4**).

Into a two-necked flask, previously dried in an oven, about 0.300 g of Pd/C 10% and approximately 50 mL of ethyl acetate were placed. After connecting the flask to an elastomer balloon containing hydrogen gas, the mixture was stirred at room temperature for 1 h in order to saturate the suspension of Pd/C with hydrogen. Then, 1.69 g (8.90 mmol) of compound **1** in 15 mL of ethyl acetate was added dropwise to the suspension, and the mixture was stirred under hydrogen at atmospheric pressure and heated by means of an oil bath at 50-60 °C while monitoring the progress of the reaction by TLC analysis (ethyl acetate/toluene/*n*-hexane, 1:1:1). At the end of the reaction, the mixture was filtered through a celite pad, and the solution was concentrated under vacuum to give 1.40 g of amine as a dark liquid. Yield:

98.2%; Rf: 0.28 (toluene/*n*-hexane/ethyl acetate, 1:1:1); ^1H NMR (300 MHz, DMSO- d_6): δ 7.16 (m, 2H, H-3 e H-7), 6.69 (d, $J = 2.28$ Hz, 1H, H-4), 6.54 (dd, $J = 8.5, 2.28$ Hz, 1H, H-6), 6.15 (d, $J = 3.05$ Hz, 1H, H-2), 4.48 (s br, 2H, NH₂), 4.06 (q, $J = 7.3$ Hz, 2H, CH₂), 1.55 (t, $J = 7.3$ Hz, 3H, CH₃) ppm; HRMS (ESI-MS, 140 eV): m/z [M+H]⁺ calculated for C₁₀H₁₃N₂⁺, 161.2231; found, 161.1593.

4.1.5 (5-Amino-1H-indol-1-yl)(phenyl)methanone (**5**).

Into a 50 mL round-bottomed flask, 1-benzoyl-5-nitroindole 0.443 g (1.67 mmol) was dissolved in 30 mL of EtOAc. Pt/C catalyst (65 mg, 15% p/p) was added under N₂ atmosphere, and then the mixture was treated with H₂ for 75 min at room temperature. The catalyst was removed by filtration on a celite pad, and the solution was concentrated under vacuum. The product was purified by silica gel chromatographic column (eluent CH₂Cl₂/EtOAc, 9:1), yielding 0.331 g of a pure yellow solid. Yield = 84%; Rf: 0.43 (eluent CH₂Cl₂/EtOAc, 9:1); mp = 252 °C; ^1H NMR (300 MHz, CDCl₃) δ 8.12 (d, $J = 8.7$ Hz, 1H, H-7), 7.66 – 7.58 (m, 2H, H-2' and H-6'), 7.52 – 7.38 (m, 3H, H-3', H-4' and H-5'), 7.11 (d, $J = 3.7$ Hz, 1H, H-2), 6.85 – 6.80 (m, 1H, H-3), 6.72 (dd, $J = 8.7, 2.2$ Hz, 1H, H-6), 6.38 (dd, $J = 3.7, 0.6$ Hz, 1H, H-3), 3.06 (s, 2H, NH₂) ppm; HRMS (ESI-MS, 140 eV): m/z [M+H]⁺ calculated for C₁₅H₁₃N₂O⁺, 237.1022; found, 237.1043.

4.1.6 (5-Amino-1H-indol-1-yl)(2-fluorophenyl)methanone (**6**).

Into a 50 mL round-bottomed flask, 0.375 g of compound **3** (1.32 mmol) were dissolved in 25 mL of EtOAc. Pt/C catalyst (60 mg, 15% p/p) was added under N₂ atmosphere, and then the mixture was treated with H₂ for 75 min at room temperature. The catalyst was removed by filtration on a celite pad, and the solution was concentrated under vacuum. The product was purified by silica gel chromatographic column (eluent CH₂Cl₂/EtOAc, 9:1), yielding 0.293 g

of a solid. Yield = 87%; Rf: 0.40 (eluent CH₂Cl₂/EtOAc, 9:1); mp = 265 °C; ¹H NMR (300 MHz, CDCl₃) δ 7.84 (m, *J* = 8.1, 1.5 Hz, 1H), 7.56 (dd, *J* = 8.3, 7.4 Hz, 1H), 7.63 (dt, *J* = 8.2, 0.5 Hz, 1H), 7.42 (m, *J* = 8.3, 1.4 Hz, 1H), 7.44 (m, *J* = 8.3, 0.4 Hz, 1H), 7.33 (dd, *J* = 8.1, 7.4 Hz, 1H), 7.30 (m, *J* = 1.9, 0.4 Hz, 1H), 6.52 (m, *J* = 8.2, 2.0 Hz, 1H), 6.33 (dd, *J* = 8.3, 1.9 Hz, 1H), 3.01 (s, 2H, NH₂) ppm; HRMS (ESI-MS, 140 eV): *m/z* [M+H]⁺ calculated for C₁₅H₁₂FN₂O⁺, 255.0928; found, 255.0912.

4.1.7 General procedure for the synthesis of acrylate derivatives 7-11. As a typical procedure, the synthesis of acrylate derivative **7** is described in detail. In a 100 mL round-bottomed flask, 0.700 g (4.37 mmol) of 3-ethyl aminoindole **4** were dissolved in 10 mL of absolute ethanol. 0.5 mL of glacial acetic acid, 0.100 g of drierite and 1.84 g (8.74 mmol) of ethyl 3-(2-fluorophenyl)-3-oxopropanoate dissolved in 2 mL of absolute ethanol were added to the solution. The mixture was refluxed for about 48 h, the reaction being monitored by TLC analysis (*n*-hexane/ethyl acetate, 1:1). At the end of the reaction, the mixture was cooled and filtered to remove the drierite; the resulting solution was evaporated to dryness under vacuum and the residue (2.47 g) purified by silica gel chromatography (d = 3 cm, l = 35 cm, 230–400 mesh, eluent *n*-hexane/ethyl acetate, 1:1) to yield 1.01 g of a brown solid.

(E,Z)-Ethyl 3-(1-ethyl-1H-indol-5-ylamino)-3-(2-fluorophenyl)acrylate (**7**).

Yield: 63%; Rf: 0.47 (*n*-hexane/ethyl acetate, 1:1); mp = 419 °C; ¹H NMR (400 MHz, DMSO-d₆): δ 10.72 (s, 1H, NH), 7.58 (m, *J* = 7.84, 5.37, 1.35 Hz, 1H, H-6'), 7.44 (m, *J* = 8.31, 7.41, 1.35 Hz, 1H, H-5'), 7.37 (d, *J* = 9.08 Hz, 1H, H-7), 7.30 (d, *J* = 3.15 Hz, 1H, H-2), 7.23 (m, *J* = 7.84, 7.41, 1.38 Hz, 1H, H-4'), 6.95 (m, *J* = 8.29, 5.31, 1.57, 1H, H-3'), 6.94 (m, *J* = 2.08 Hz, 1H, H-4), 6.65 (dd, *J* = 8.71, 2.08 Hz, 1H, H-6), 6.27 (dd, *J* = 3.19, 0.69 Hz, 1H, H-3), 4.83 (s, 1H, CHCOOCH₂CH₃), 4.16 (q, *J* = 6.92 Hz, 2H, COOCH₂CH₃), 3.84 (q, *J* = 7.64 Hz, 2H, NCH₂CH₃), 1.25 (t, *J* = 6.92 Hz, 3H, COOCH₂CH₃), 1.13 (t, *J* = 7.67 Hz, 3H,

NCH₂CH₃), ppm; HRMS (ESI-MS, 140 eV): m/z [M+H]⁺ calculated for C₂₁H₂₂FN₂O₂⁺, 353.1660; found, 353.1688.

(E,Z)-Ethyl 3-(1-ethyl-1H-indol-5-ylamino)-3-(3-fluorophenyl)acrylate (8).

Compound **8** was prepared as for compound **7** by reacting 1.84 g (8.74 mmol) of ethyl 3-(3-fluorophenyl)-3-oxopropanoate with 0.700 g (4.37 mmol) of previously prepared compound **4**, yielding 2.76 g of crude product, which was purified by silica gel column chromatography (d = 3 cm, l = 35 cm, 230–400 mesh, eluent *n*-hexane/ethyl acetate, 1:1) to yield 1.07 g of a brown liquid. Yield: 67%; R_f: 0.47 (*n*-hexane/ethyl acetate, 1:1); ¹H NMR (400 MHz, DMSO-d₆): δ 10.68 (s, 1H, NH), 7.46 (m, J = 7.75, 1.52 Hz, 1H, H-6'), 7.44 (m, J = 8.21, 7.73, 1H, H-5'), 7.37 (d, J = 9.08 Hz, 1H, H-7), 7.30 (d, J = 3.15 Hz, 1H, H-2), 7.19 (m, 1H, H-2'), 7.14 (m, 1H, H-4'), 6.94 (m, J = 2.08 Hz, 1H, H-4), 6.65 (dd, J = 8.71, 2.08 Hz, 1H, H-6), 6.23 (dd, J = 3.19, 0.69 Hz, 1H, H-3), 4.89 (s, 1H, CHCOOCH₂CH₃), 4.12 (q, J = 6.92 Hz, 2H, COOCH₂CH₃), 3.83 (q, J = 7.64 Hz, 2H, NCH₂CH₃), 1.25 (t, J = 6.92 Hz, 3H, COOCH₂CH₃), 1.18 (t, J = 7.67 Hz, 3H, NCH₂CH₃) ppm; HRMS (ESI-MS, 140 eV): m/z [M+H]⁺ calculated for C₂₁H₂₂FN₂O₂⁺, 353.1660; found, 353.1645.

(E,Z)-Ethyl 3-(1-ethyl-1H-indol-5-ylamino)-3-(4-fluorophenyl)acrylate (9).

Compound **9** was prepared as for compound **7** by reacting 1.84 g (8.74 mmol) of ethyl 3-(4-fluorophenyl)-3-oxopropanoate with 0.700 g (4.37 mmol) of previously prepared compound **4**, yielding 2.60 g of crude product, which was purified by silica gel column chromatography (d = 3 cm, l = 35 cm, 230–400 mesh, eluent *n*-hexane/ethyl acetate, 1:1) to yield 1.12 g of a yellow liquid. Yield: 70%; R_f: 0.69 (*n*-hexane/ethyl acetate, 1:1); ¹H NMR (400 MHz, DMSO-d₆): δ 10.44 (s, 1H, NH), 7.97 (m, J = 5.65, 3.27, 2H, H-2' and H-6'), 7.44 (m, J = 8.90, 3.25, 2.20 Hz, 2H, H-3' and H-5'), 7.35 (d, J = 9.08 Hz, 1H, H-7), 7.29 (d, J = 3.15 Hz, 1H, H-2), 6.98 (m, J = 2.08 Hz, 1H, H-4), 6.66 (dd, J = 8.71, 2.08 Hz, 1H, H-6), 6.28 (dd, J = 3.19, 0.69 Hz, 1H, H-3), 4.85 (s, 1H, CHCOOCH₂CH₃), 4.14 (q, J = 6.92 Hz, 2H,

COOCH₂CH₃), 3.76 (q, *J* = 7.64 Hz, 2H, NCH₂CH₃), 1.24 (t, *J* = 6.92 Hz, 3H, COOCH₂CH₃), 1.14 (t, *J* = 7.67 Hz, 3H, NCH₂CH₃) ppm; HRMS (ESI-MS, 140 eV): *m/z* [M+H]⁺ calculated for C₂₁H₂₂FN₂O₂⁺, 353.1660; found, 353.1656.

(E,Z)-Ethyl-3-[(1-benzoylindol-5-ylamino)-3-(3-fluorophenyl)prop-2-enoate (**10**).

Compound **10** was prepared as for compound **7** by reacting 0.660 mL (3.66 mmol) of ethyl 3-(3-fluorophenyl)-3-oxopropanoate with 0.864 g (3.66 mmol) of previously prepared compound **5**, yielding 1.85 g of crude product, which was purified by silica gel column chromatography (d = 3 cm, l = 35 cm, 230–400 mesh, eluent petroleum ether/acetone 85:15) to yield 0.540 g of a yellow solid. Yield: 35%; *R_f*: 0.69 (eluent petroleum ether/acetone 85:15); mp = 396 °C; ¹H NMR (300 MHz, DMSO) δ 10.23 (s, 1H, NH), 8.06 (d, *J* = 8.8 Hz, 1H, H-7), 7.70 (m, 2H, H-2'' and H-6''), 7.65 (dt, *J* = 2.8, 2.0 Hz, 1H, H-4'), 7.60 – 7.52 (m, 2H, H-3'' and H-5''), 7.40 – 7.31 (m, 1H, H-2'), 7.29 (d, *J* = 3.8 Hz, 1H, H-4), 7.24 – 7.15 (m, 3H, H-4'', H-5' and H-6'), 7.07 (d, *J* = 2.1 Hz, 1H, H-2), 6.84 (dd, *J* = 8.8, 2.2 Hz, 1H, H-6), 6.56 (d, *J* = 3.4 Hz, 1H, H-3), 5.00 (s, 1H, CHCOOCH₂CH₃), 4.15 (q, *J* = 7.1 Hz, 2H, COOCH₂CH₃), 1.24 (t, *J* = 7.1 Hz, 3H, COOCH₂CH₃) ppm; HRMS (ESI-MS, 140 eV): *m/z* [M+H]⁺ calculated for C₂₆H₂₂FN₂O₃⁺, 429.1605; found, 429.1612.

(E,Z)-Ethyl-3-[(2-fluoro-1-benzoylindol-5-ylamino)-3-phenyl-prop-2-enoate (**11**).

Compound **11** was prepared as for compound **7** by reacting 0.869 mL (5.11 mmol) of ethyl-benzoyl-acetate with 0.866 g (3.41 mmol) of previously prepared compound **6**, yielding 1.65 g of crude product, which was purified by silica gel column chromatography (d = 3 cm, l = 35 cm, 230–400 mesh, eluent petroleum ether/acetone 85:15) to yield 0.456 g of a yellow solid. Yield: 31%; *R_f*: 0.77 (eluent petroleum ether/acetone 90:10); mp = 409 °C; ¹H NMR (300 MHz, DMSO) δ 10.29 (s, 1H, NH), 8.01 (d, *J* = 8.1 Hz, 1H, H-7), 7.65 (m, 2H, H-2' and H-6'), 7.57 (dt, *J* = 2.8, 2.0 Hz, 1H, H-4''), 7.60 – 7.58 (m, 2H, H-3' and H-5'), 7.40 – 7.38 (m, 1H, H-2''), 7.28 (d, *J* = 3.2 Hz, 1H, H-4), 7.23 – 7.10 (m, 3H, H-4', H-5'' and H-6''), 7.02 (d, *J*

= 2.1 Hz, 1H, H-2), 6.80 (dd, $J = 8.8, 2.21$ Hz, 1H, H-6), 6.66 (d, $J = 3.3$ Hz, 1H, H-3), 5.02 (s, 1H, $CHCOOCH_2CH_3$), 4.12 (q, $J = 7.0$ Hz, 2H, $COOCH_2CH_3$), 1.26 (t, $J = 7.0$ Hz, 3H, $COOCH_2CH_3$) ppm; HRMS (ESI-MS, 140 eV): m/z $[M+H]^+$ calculated for $C_{26}H_{22}FN_2O_3^+$, 429.1609; found, 429.1626.

4.1.8 General procedure for the synthesis of phenylpyrroloquinolinones (**12-15**).

As a typical procedure, the synthesis of the phenylpyrroloquinolinone derivative **12** is described in detail. In a two-necked round-bottomed flask, 7 mL of diphenyl ether was heated to boiling. 1.03 g (2.8 mmol) of acrylate derivative **7** was then added, and the resulting mixture was refluxed for 15 min. After cooling to room temperature, 20 mL of diethyl ether was added, and the mixture was left for 12 h. Then the separated precipitate was collected by filtration and washed many times with diethyl ether. The crude product (0.530 g) was purified by flash column chromatography (eluent chloroform/methanol, 9:1), obtaining 0.220 g of final pure compound.

3-Ethyl-7-(2-fluorophenyl)-3H-pyrrolo[3,2-f]quinolin-9(6H)-one (**12**).

Yield: 26%; R_f: 0.53 (light blue fluorescent spot, chloroform/methanol 9:1); mp = 301 °C; ¹H NMR (400 MHz, DMSO-d₆) δ 11.64 (s, 1H, NH), 7.93 (d, $J = 9.06$ Hz, 1H, H-4), 7.90 – 7.85 (m, 2H, H-1 and H-6'), 7.69 – 7.51 (m, 4H, H-2, H-3', H-5' and H-5), 7.51 (m, 1H, H-4'), 6.39 (s, 1H, H-8), 4.32 (q, $J = 6.51$ Hz, 2H, NCH_2CH_3), 1.41 (t, $J = 6.51$ Hz, 3H, NCH_2CH_3) ppm; ¹³C NMR (101 MHz, DMSO-d₆) δ 178.38 ppm (C-9), 154.54 (C-6), 141.98 (d, $J=246.83$ Hz, C-2'), 133.12 (d, $J=21.52$ Hz, C-1'), 132.26 (C-3a), 131.85 (C-7), 131.42 (C-5a), 130.75 (C-2), 129.78 (d $J=20.97$ Hz, C-3' and C-5'), 129.36 (d, $J=3.24$ Hz, C-4'), 128.90 (d, $J=7.94$ Hz, C-6'), 128.14 (C-9b), 118.46 (C-9a), 116.49 (C-4), 116.27 (C-5), 109.03 (C-8), 104.52 (C-1), 41.38 (NCH_2CH_3), 16.74 (NCH_2CH_3) ppm; IR (KBr): $\nu = 3422.38$ (NH), 3022 (aromatic C-H), 2901.12 (aliphatic C-H), 1608.38 (C=O), 1509.10 (C=C), 1228.67 (C-F) cm⁻¹; UV-Vis

(H₂O): 273 nm (A = 0.473 mAU), 342 nm (A = 0.297 mAU); fluorescence (H₂O): λ_{exc} = 342 nm, λ_{ems} = 484.02 nm; ESI-MS: m/z [M+H]⁺ calculated for C₁₉H₁₆FN₂O⁺, 307.1241; found, 307.1287; RP-C18 HPLC: t_{R} = 13.27 min, 95.07%

3-Ethyl-7-(3-fluorophenyl)-3H-pyrrolo[3,2-f]quinolin-9(6H)-one (13).

Compound **13** was prepared as described for compound **12** by reacting 1.07 g (2.92 mmol) of the appropriate phenyl-acrylate derivative **8** to yield 0.836 g of a raw solid, which was purified by flash column chromatography (eluent chloroform/methanol, 9:1) to yield 0.332 g of final compound. Yield: 37%; R_f: 0.53 (light blue fluorescent spot, chloroform/methanol, 9:1); mp = 303 °C; ¹H NMR (400 MHz, DMSO-d₆) δ 8.00 (dd, J=9.35 Hz and J=0.70 Hz, 1H, H-4), 7.67 (dd, J=2.92 Hz and J=0.72 Hz, 1H, H-1), 7.59 (d, J=9.35 Hz, 1H, H-5), 7.57 (m, 5H, H-2', H-4', H-5', H-6'), 7.57 (m, 1H, H-2), 6.04 (s, 1H, H-8), 4.37 (q, J=7.20 Hz, 2H, NCH₂CH₃), 1.42 (t, J=7.20 Hz, 3H, NCH₂CH₃) ppm; ¹³C NMR (101MHz, DMSO-d₆) δ : 178.25 (C-9), 163.27 (d, J=247.72 Hz, C-3'), 137.97 (C-3a), 135.83 (C-5a), 131.92 (d, J=7.93 Hz, C-1'), 131.43 (C-7), 129.69 (d, J= 3.14 Hz, C-4'), 128.61 (d, J=21.24 Hz, C-2' and C-6'), 124.36 (C-2 and C-9b), 123.85 (d, J=7.36 Hz, C-5'), 118.59 (C-9a), 116.42 (C-4), 113.78 (C-8), 108.67 (C-5), 104.68 (C-1), 41.50 (NCH₂CH₃), 16.82 (NCH₂CH₃) ppm; IR (KBr): ν = 3427.83 (NH), 3027 (aromatic C-H), 2928.07 (aliphatic C-H), 1602.79 (C=O), 1508.25 (C=C), 1222.76 (C-F) cm⁻¹; UV-Vis (H₂O): 273 nm (A = 0.326 mAU), 344 nm (A = 0.202 mAU); fluorescence (H₂O): λ_{exc} = 344 nm, λ_{ems} = 492.98 nm; ESI-MS: m/z [M+H]⁺ calculated for C₁₉H₁₆FN₂O⁺, 307.1241; found, 307.1264; RP-C18 HPLC: t_{R} = 13.15 min, 96.25%.

3-Ethyl-7-(4-fluorophenyl)-3H-pyrrolo[3,2-f]quinolin-9(6H)-one (14).

Compound **14** was prepared as described for compound **12** by reacting 1.12 g (3.05 mmol) of the appropriate phenylacrylate derivative **9** to yield 0.340 g of a raw solid that was purified by flash column chromatography (eluent chloroform/methanol, 9:1) to yield 0.320 g of final compound. Yield: 39%; R_f: 0.59 (light blue fluorescent spot, chloroform/methanol, 9:1); mp =

308 °C; ^1H NMR (400 MHz, DMSO- d_6) δ 11.66 (s, 1H, NH), 7.93 (m, $J = 5.46, 3.24$ Hz, 2H, H-2' and H-6'), 7.90 (d, $J=8.96$ Hz, 1H, H-4), 7.57 (d, $J = 8.92$ Hz, 1H, H-5), 7.52 (d, $J = 2.66$ Hz, 1H, H-1), 7.50 (d, $J = 2.82$ Hz, 1H, H-2), 7.42 (m, $J = 8.86, 3.19, 2.19$ Hz, 2H, H-3' and H-5'), 6.47 (s, 1H, H-8), 4.32 (q, $J = 7.21$ Hz, 2H, NCH_2CH_3), 1.41 (t, $J = 7.22$ Hz, 3H, NCH_2CH_3) ppm; ^{13}C NMR (101 MHz, DMSO- d_6) δ 178.69 (C-9), 163.97 (d, $J=247.32$ Hz, C-4'), 147.32 (C-7), 137.21 (C-5a), 131.91 (C-3a), 130.51 (d, $J=8.63$ Hz, C-2' and C-6'), 128.91 (C-2), 123.90 (C-9a and C-9b), 118.74 (d, $J=2.31$ Hz, C-1'), 116.73 (d, $J=21.80$ Hz, C-3' and C-5'), 116.33 (C-4), 113.13 (C-5), 109.02 (C-8), 104.59 (C-1), 41.43 (NCH_2CH_3), 16.78 (NCH_2CH_3) ppm; IR (KBr): $\nu = 3422.31$ (NH), 3078 (aliphatic C-H), 2930.57 (aliphatic C-H), 1609.22 (C=O), 1508.23 (C=C), 1220.20 cm^{-1} (C-F); UV-Vis (H_2O): 269 nm ($A = 0.248$ mAU), 352.97 nm ($A = 0.165$ mAU); fluorescence (H_2O): $\lambda_{\text{exc}} = 352.97$ nm, $\lambda_{\text{ems}} = 484.02$ nm; HRMS (ESI-MS, 140 eV): m/z $[\text{M}+\text{H}]^+$ calculated for $\text{C}_{19}\text{H}_{16}\text{FN}_2\text{O}^+$, 307.1241; found, 307.1272; RP-C18 HPLC: $t_{\text{R}} = 12.95$ min, 97.05%.

3-Benzoyl-7-(3-fluorophenyl)-6H-pyrrolo[3,2-f]quinolin-9-one (15).

Compound **15** was prepared as described for compound **12** by reacting 0.150g (3.05 mmol) of the appropriate phenyl-acrylate derivative **10** to yield 0.080 g of final compound. Yield: 56%; R_f : 0.59 (light blue fluorescent spot, chloroform/methanol, 9:1); mp = 329 °C; ^1H NMR (300 MHz, DMSO) δ 6.51 (s, 1H, H-8), 7.43 (t, $J = 8.5$ Hz, 1H), 7.52 (d, $J = 3.6$ Hz, 1H), 7.68 – 7.60 (m, 3H, H-3', H-4' and H-5') 7.87 – 7.70 (m, 7H, H-2', H-6',), 8.61 (d, $J = 9.1$ Hz, 1H, H-4), 11.90 (s, 1H, NH) ppm; ^{13}C NMR (101 MHz, DMSO- d_6) δ 179.80 (CO), 165.20 (NCO), 163.04 (d, $J=248.16$ Hz, C-3'), 135.57 (C-3a), 135.12 (C-5a), 133.65 (C-7), 130.64 (C-4''), 130.12 (d, $J=7.91$ Hz, C-1'), 129.99 (d, $J= 3.28$ Hz, C-4'), 129.96 (C-3'' and C-5''), 128.11 (d, $J=21.24$ Hz, C-2' and C-6'), 127.64 (C-2'' and C-6''), 124.19 (C-2 and C-9b), 124.02 (d, $J=7.32$ Hz, C-5'), 120.45 (C-4), 120.14 (C-9a), 117.02 (C-5), 110.41 (C-1), 107.03

(C-8) ppm; UV-Vis (H₂O): 275 nm (A = 0.568 mAU); fluorescence (H₂O): λ_{exc} = 275 nm, λ_{ems} = 541 nm; HRMS (ESI-MS, 140 eV): m/z [M+H]⁺ calculated for C₂₄H₁₆FN₂O₂⁺, 383.1190; found, 383.1175; RP-C18 HPLC: t_R = 20.50 min, 95.62%.

4.1.8 2-Fluorobenzoyl chloride (**17**).

2.0 g of 2-fluorobenzoic acid (14.27 mmol) was placed in a 50 mL round-bottomed flask, and 7 mL of thionyl chloride was added. The mixture was refluxed at 80 °C for 2 h and concentrated under reduced pressure, and the residue was co-evaporated with toluene (10 mL) 3 times to obtain 0.910 g of a yellow oil. The compound was used for the next step without further purification. Yield = 40%; ¹H NMR signals were compatible with data reported in the literature.

*Synthesis of 7-phenyl-3H-pyrrolo[3,2-f]quinolin-9-yl 2-fluorobenzoate (**18**) and 3-(2-fluorobenzoyl)-7-phenyl-6H-pyrrolo[3,2-f]quinolin-9-one (**19**).*

Into a two-necked 50 mL round-bottomed flask, 0.060 g (2.54 mmol, 3 eq.) of NaH, 60% dispersion in mineral oil, was placed and washed with toluene (3 x 10 mL). With stirring, a solution of 7-phenyl- 3H,6H-pyrrolo[3,2-f]quinolin-9-one (**16**), (prepared as previously reported in [7]), 0.220 g (0.85 mmol, 1 eq.) in 7 mL of anhydrous DMF, was dropped into the flask. After 40 min at room temperature, a solution of 2-fluorobenzoyl chloride, 0.40 g (2.54 mmol, 3 eq.) in 2 mL dry DMF, was added, and the reaction mixture was stirred for 2 h. The reaction was monitored by TLC analysis (eluent chloroform/methanol, 9:1). At the end of the reaction, 25 mL of water was added, and the reaction mixture was extracted with EtOAc (3 x 50 mL). The combined organic phases were washed with water and brine, dried over anhydrous Na₂SO₄ and concentrated under vacuum to yield a crude brown solid (1.44 g). This crude product was purified with flash column chromatography (chloroform/methanol, 9:1), yielding 0.236 g of compound **18** and 0.070 g of desired compound **19**. Compound **18**: yield

78%; R_f: 0.70 (light blue fluorescent spot, chloroform/methanol, 9:1); mp = 324 °C; ¹H NMR (400 MHz, DMSO-d₆) δ 11.90 (s, 1H, NH), 8.46 (t, J=6.86 Hz, 1H, H-4), 8.34 (m, 1H, H-6''), 8.17 (d, J=9.19 Hz, 1H, H-5), 8.02 (m, 2H, H-2' and H-6'), 7.86 (d, J=3.21 Hz, 1H, H-2), 7.75 - 7.85 (m, 3H, H-3'', H-4'' and H-5''), 7.71 (m, 2H, H-3' and H-5'), 7.70 (m, 1H, H-4'), 7.67 (s, 1H, H-8), 7.42 (dd, J=2.99 Hz and J=0.65 Hz, 1H, H-1) ppm; ¹³C NMR (101 MHz, DMSO-d₆) δ 176.63 (CO), 169.98 (C-9), 164.62 (d, J=245.27 Hz, C-2''), 151.15 (C-7), 138.72 (d, J=21.62 Hz, C-1''), 137.87 (C-5a), 133.62 (d, J=7.82 Hz, C-4''), 132.61 (C-1'), 132.58 (C-3a), 132.12 (C-4'), 131.44 (d, J=7.47 Hz, C-6''), 130.95 (C-2), 129.94 (d, J=2.61 Hz, C-5''), 129.83 (C-3' and C-5'), 129.05 (C-2' and C-6'), 120.68 (C-9b), 120.13 (C-4), 118.24 (d, J=21.82 Hz, C-3''), 114.10 (C-9a), 113.22 (C-5), 105.40 (C-1), 105.19 (C-8) ppm; IR (KBr): ν = 3301 cm⁻¹ (NH), 3024.54 cm⁻¹ (aromatic C-H), 2961.89 cm⁻¹ (aliphatic C-H), 1458.09 cm⁻¹ (C=C), 1736.10 cm⁻¹ (COO), 1239.51 cm⁻¹ (C-F); UV-Vis (H₂O): 269 nm (A = 0.640), 376 nm (A = 0.393); fluorescence (H₂O): λ_{exc} = 376 nm, λ_{em} = 473.93 nm; HRMS (ESI-MS, 140 eV): m/z [M+H]⁺ calculated for C₂₄H₁₆FN₂O₂⁺, 383.119; found, 383.1261; RP-C18 HPLC: t_R = 15.44 min, 98 %; **Compound 19**: yield: 22%; R_f: 0.60 (light blue fluorescent spot, chloroform/methanol, 9:1); mp = 163°C; ¹H NMR (400 MHz, DMSO-d₆) δ 11.95 (m, 1H, NH), 8.65 (d, J = 9.12 Hz, 1H, H-4), 7.87 (m, 2H, H-2' and H-6'), 7.86 (m, 1H, H-5''), 7.82 (m, J = 2.95 Hz, 1H, H-2), 7.80 (m, J = 2.84 Hz, 1H, H-1), 7.74 (m, 1H, H-4'), 7.60 (m, 2H, H-3' and H-5'), 7.50 (d, J = 9.12 Hz, 1H, H-5), 7.46 (m, 1H, H-3''), 7.39 (m, J = 1.60 Hz, 1H, H-6''), 7.26 (m, 1H, H-4''), 6.45 (s, 1H, H-8) ppm; ¹³C NMR (101 MHz, DMSO-d₆) δ 178.50 (CO), 164.93 (NCO), 160.27 (C-7), 158.93 (d, J=249.32, C-2''), 149.44 (C-5a), 140.27 (d, J=22.78 Hz, C-1''), 139.14 (C-3a), 135.17 (d, J=8.76 Hz, C-4''), 134.48 (C-1), 134.24 (C-4'), 132.34 (d, J=1.30 Hz, C-5''), 130.71 (d, J=7.82 Hz, C-6''), 129.52 (C-3' and C-5'), 128.51 (C-2), 127.94 (C-2' and C-6'), 120.54 (C-9b), 120.54 (C-4), 119.84 (C-9a), 117.25 (d, J=23.04

Hz, C-3''), 116,56 (C-5), 111.16 (C-1), 109.12 (C-8) ppm; IR (KBr): $\nu = 3430.03 \text{ cm}^{-1}$ (NH), 3067.39 cm^{-1} (aromatic C-H), 2964 cm^{-1} (aliphatic C-H), 1687 cm^{-1} (C=O), 1547 cm^{-1} (C=C), 1351.18 cm^{-1} (C-F); UV-Vis (H₂O): 280 nm (A = 0.989), 346.42 nm (A = 0.803); fluorescence (H₂O): $\lambda_{\text{exc}}=346.42 \text{ nm}$, $\lambda_{\text{em}}=500.00 \text{ nm}$; HRMS (ESI-MS, 140 eV): m/z [M+H]⁺ calculated for C₂₄H₁₆FN₂O₂⁺, 383.119; found, 383.1261; RP-C18 HPLC: $t_{\text{R}} = 15.24 \text{ min}$, 96.5 %.

4.2 Biological assays

4.2.1 Cell growth conditions and antiproliferative assay

Human T-cell leukemia (Jurkat, DND-41, and CEM), B-cell leukemia (RS4;11) and promyelocytic leukemia (HL-60) cells were grown in RPMI-1640 medium (Gibco, Milano, Italy). Human breast adenocarcinoma (MCF-7, MDA-MB-231, MDA-MB-468), cervix carcinoma (HeLa), melanoma (A375 and A2058) and colon adenocarcinoma (HT-29) cells were grown in DMEM medium (Gibco, Milano, Italy), all supplemented with 115 units/mL penicillin G (Gibco, Milano, Italy), 115 $\mu\text{g/mL}$ streptomycin (Invitrogen, Milano, Italy), and 10% fetal bovine serum (Invitrogen, Milano, Italy). Stock solutions (10 mM) of the different compounds were obtained by dissolving them in DMSO. Individual wells of a 96-well tissue culture microtiter plate were inoculated with 100 μL of complete medium containing 8×10^3 cells. The plates were incubated at 37 °C in a humidified 5% CO₂ incubator for 18 h prior to the experiments. After medium removal, a 100 μL aliquot of fresh medium containing the test compound at varying concentrations was added to each well in triplicate and incubated at 37 °C for 72 h. Cell viability was assayed by the MTT test as previously described [28]. The GI₅₀ was defined as the compound concentration required to inhibit cell proliferation by 50%.

CEM^{vbl-100} cells are a multidrug-resistant line selected against vinblastine and were a kind gift of Dr. G. Arancia (Istituto Superiore di Sanità, Rome, Italy). They were grown in RPMI-1640 medium supplemented with 100 ng/mL of vinblastine.

Peripheral blood lymphocytes (PBL) from healthy donors were obtained by separation on a Lymphoprep (Fresenius KABI Norge AS) gradient. After extensive washing, cells were resuspended (1.0×10^6 cells/mL) in RPMI-1640 with 10% fetal bovine serum and incubated overnight. For cytotoxicity evaluations in proliferating PBL cultures, non-adherent cells were resuspended at 5×10^5 cells/mL in growth medium containing 2.5 μ g/mL PHA (Irvine Scientific). Different concentrations of the test compounds were added, and viability was determined 72 h later by the MTT test. For cytotoxicity evaluations in resting PBL cultures, non-adherent cells were resuspended (5×10^5 cells/mL) and treated for 72 h with the test compounds, as described above.

4.2.2 Effects on tubulin polymerization and on colchicine binding to tubulin

To evaluate the effect of the compounds on tubulin assembly *in vitro* [18], varying concentrations of compounds were preincubated with 10 μ M bovine brain tubulin in 0.8 M monosodium glutamate (from a 2 M stock solution adjusted to pH 6.6 with HCl) for 15 min at 30 °C and then cooled to 0 °C. After addition of 0.4 mM GTP (final concentration), the mixtures were transferred to 0 °C cuvettes in a recording spectrophotometer equipped with an electronic temperature controller and warmed to 30 °C. Tubulin assembly was followed turbidimetrically at 350 nm. The IC₅₀ was defined as the compound concentration that inhibited the extent of assembly by 50% after a 20 min incubation. The ability of the test compounds to inhibit colchicine binding to tubulin was measured as described [18], with the reaction mixtures containing 1 μ M tubulin, 5 μ M [³H]colchicine and 5 μ M test compound.

4.2.3 Flow cytometric analysis of cell cycle distribution

5×10^5 HeLa cells were treated with different concentrations of the test compounds for 24 h. After the incubation period, the cells were collected, centrifuged, and fixed with ice-cold ethanol (70%). The cells were then treated with lysis buffer containing RNase A and 0.1% Triton X-100 and stained with PI. Samples were analyzed on a Cytomic FC500 flow cytometer (Beckman Coulter). DNA histograms were analyzed using MultiCycle for Windows (Phoenix Flow Systems).

4.2.4 Apoptosis assay

Cell death was determined by flow cytometry of cells double stained with annexin V/FITC and PI. The Coulter Cytomics FC500 (Beckman Coulter) was used to measure the surface exposure of PS on apoptotic cells according to the manufacturer's instructions (Annexin-V Fluos, Roche Diagnostics).

4.2.5 Analysis of mitochondrial potential and ROS

The mitochondrial membrane potential was measured with the lipophilic cation JC-1 (Molecular Probes, Eugene, OR, USA), while the production of ROS was followed by flow cytometry using the fluorescent dye H₂DCFDA (Molecular Probes), as previously described [30].

4.2.6 Western blot analysis

HeLa cells were incubated in the presence of **12** and, after different times, were collected, centrifuged, and washed two times with ice cold phosphate buffered saline (PBS). The pellet was then resuspended in lysis buffer. After the cells were lysed on ice for 30 min, lysates were centrifuged at 15000 x g at 4 °C for 10 min. The protein concentration in the supernatant was determined using the BCA protein assay reagents (Pierce, Italy). Equal amounts of protein (10 µg) were resolved using sodium dodecyl sulfate-polyacrylamide gel electrophoresis (SDS-PAGE) (Criterion Precast, BioRad, Italy) and transferred to a PVDF Hybond-P membrane (GE Healthcare). Membranes were blocked with a bovine serum albumin solution (5% in Tween PBS 1X), and the membranes were gently rotated overnight at 4 °C. Membranes were then incubated with primary antibodies against Bcl-2, PARP, caspase-3, H2AX, cdc25c, cyclin B, p-cdc2^{Tyr15}, Mcl-1 (all from Cell Signaling) and β-actin (Sigma-Aldrich) for 2 h at room temperature. Membranes were next incubated with peroxidase labeled secondary antibodies for 60 min. All membranes were visualized using ECL Select (GE Healthcare), and images were acquired using an Uvitec-Alliance imaging system (Uvitec, Cambridge, UK). To ensure equal protein loading, each membrane was stripped and reprobed with anti-actin antibody.

4.2.7 *In vivo* animal studies.

Animal experiments were approved by our institutional animal ethics committee (OPBA, Organismo Preposto al Benessere degli Animali, Università degli Studi di Brescia, Italy) and were executed in accordance with national guidelines and regulations. Procedures involving animals and their care conformed with institutional guidelines that comply with national and international laws and policies (EEC Council Directive 86/609, OJ L 358, 12 December 1987) and with “ARRIVE” guidelines (Animals in Research Reporting *In Vivo* Experiments). Six-week old C57BL/6 mice (Envigo) were injected subcutaneously into the dorsolateral flank

with 2.5×10^5 BL6-B16 murine melanoma cells in 200 μL total volume of PBS. When tumors were palpable, animals were treated intraperitoneally every other day with different doses of test compounds dissolved in 50 μL of DMSO. Tumors were measured in two dimensions, and tumor volume was calculated according to the formula $V=(D \times d^2)/2$, where D and d are the major and minor perpendicular tumor diameters, respectively.

4.3 In vitro drug metabolism studies

4.3.1 Metabolite profiling of compound 20 in human liver microsomes. The incubation mixtures (final volume, 0.2 mL) contained 10 μM compound **20**, 0.5 mg of protein/mL of pooled, mixed-gender, human liver microsomes (HLMs; catalog No. H0610, lot No. 120097; Xenotech LLC, Lenexa, USA), 1 mM NADPH (Santa Cruz Biotechnologies, Inc, Dallas, USA), and 0.1 M KH_2PO_4 (pH 7.4). The reaction was started following a 3-min thermal equilibration at 37°C by adding the microsomes, conducted at 37°C under aerobic conditions, and terminated after 60 min by adding 0.2 mL of ice-cold acetonitrile. Control incubations were conducted in the absence of NADPH. After protein removal by centrifugation at 20,000g for 10 min (4 °C), an aliquot of the supernatant was analyzed by HPLC with fluorescence detection, and major fluorescent peaks were collected manually and subjected to mass spectrometry as described below.

4.3.2 Metabolic stability of compounds 12-15 and 19-21 in human liver microsomes.

To compare the susceptibility of **12**, **13**, **14**, **15**, **19**, **20** and **21** to liver microsomal oxidative metabolism, each test compound (final concentration, 10 μM) was incubated in a mixture (total volume, 0.2 mL) containing 0.1 M KH_2PO_4 (pH 7.4), 0.5 mg/mL (compounds **12-14** or **20**) or 1 mg/mL (compounds **15**, **19** and **21**) of pooled, mixed-gender HLMs (catalog No. H0610, lot No. 120097; Xenotech LLC), and 1 mM NADPH (Santa Cruz Biotechnologies,

Inc.). The reactions were started following a 3-min thermal equilibration at 37 °C by adding the microsomes and terminated by adding 0.2 mL of ice-cold acetonitrile after 0- or 60- (compounds **15**, **19** and **21**), or after 0-, 2-, 5-, 15-, or 30-min (compounds **12-14** and **20**) incubations at 37 °C. These incubation conditions were established based on preliminary single-time point (60 min) experiments indicating significant depletion of compounds **12-14** and **20**, but not **15**, **19** and **21**, in incubation mixtures containing HLMs (0.5 mg/mL) and NADPH (1 mM). Zero- and 30-min control incubations were performed in the absence of NADPH, as well as in the absence of both HLMs and NADPH (buffer-only incubations). Samples were then centrifuged (4 °C) at 20,000 *g* for 10 min, and aliquots of the supernatants were analyzed for the disappearance of test compounds by HPLC with fluorescence detection, as described below.

4.3.3 Chemical inhibition studies. To assess the role of CYP in liver microsomal metabolism of compounds **12-14** and **20**, each test compound (10 µM) was incubated at 37(add space)°C for 0 and 15 min in 0.2 mL of 0.1 M KH₂PO₄ (pH 7.4) containing 0.5 mg/mL pooled, mixed-gender HLMs (catalog No. H0610, lot. No. 0810472, Xenotech LLC), 1 mM NADPH (Santa Cruz Biotechnologies, Inc.), and the non-selective CYP inhibitor quercetin (100 µM; [13-15]); the incubation protocol and sample preparation for HPLC analysis were the same as described above. Control incubations were carried out in the absence of quercetin.

4.3.4 HPLC analysis. All chromatographic analyses were carried out using an HPLC system (Agilent Technologies Inc., formerly Hewlett-Packard Co, Palo Alto, USA) equipped with of a series 1200 degasser, a series 1100 quaternary pump, a series 1100 autosampler, a series 1100 column oven, and a series 1200 fluorescence detector; data were collected and integrated using the Agilent ChemStation software. Chromatographic conditions were as follows: column, Agilent Zorbax SB C18 (4.6 x 75 mm, 3.5 µm; Agilent Technologies Inc.;

analysis of compounds **12-15**, and **21**), Symmetry Shield RP18 (4.6 x 150 mm, 5 μ m; Waters Corp., Milford, USA; analysis of the metabolic stability of compound **20**), or Symmetry C8 (4.6 \times 250 mm, 5 μ m; Waters Corp.; metabolic profile analysis of compound **20**); mobile phase, 0.1% formic acid in water (solvent A), and 0.1% formic acid in acetonitrile (solvent B); elution program, isocratic elution with 95% solvent A for 2 min, linear gradient from 5 to 40% solvent B in 8 min, followed by a further linear gradient from 40 to 60% solvent B in 2 min, and an isocratic elution with 60% solvent B for 7 min; post-run time, 5 min; flow rate, 1.0 mL/min; injection volume, 50 μ L; column temperature, 30 $^{\circ}$ C; detection, fluorescence (excitation wavelength, 344 nm; emission wavelength, 493 nm). Under the above conditions, the retention times were 11.6, 11.5, 11.5, 13.8, 13.4, and 13.5 min for **12**, **13**, **14**, **15**, **19**, and **21**, respectively; the retention time for compound **20** was 12.9 (Symmetry C8 column) or 11.3 min (Symmetry Shield RP18 column)..

4.3.5 Mass spectrometry. Collected HPLC peak fractions were subjected to electrospray ionization time-of-flight mass spectrometry (ESI-TOF-MS) performed on a Xevo G2-S QToF (Waters Corp.). The mass spectrometer operated under the following conditions: electrospray in positive ion mode (ES+); source temperature, 100 $^{\circ}$ C; desolvation gas temperature, 450 $^{\circ}$ C; capillary voltage, 2.0 kV; sampling cone voltage, 40 V. Data were collected by full scan mode (scan range of m/z , 50-2000) and evaluated by the MassLynx software (Waters Corp.).

4.3.6 Data analysis. Metabolic stability of each test compound, expressed as percent of compound remaining (mean \pm SD; $n = 3$), was calculated by comparing the corresponding chromatographic peak area at each time point relative to that at time 0 min. The half-life of compounds **12-14** and **20** in NADPH-supplemented human liver microsomal incubations was calculated as $t_{1/2} = 0.693/k$, where k is the slope of the line obtained by linear regression of the natural logarithmic percentage (Ln %) of compound remaining versus incubation time (min).

Results of the chemical inhibition studies were analyzed by the Student's t-test.

4.4 Molecular modelling

All the synthesized compounds in Table X were built and their partial charges calculated after semi-empirical (PM6) energy minimization using the MOE2018 software [39, 40]. The molecular docking studies are based on the protocol recently reported on this target [11] obtained by a benchmark of different protein/scoring protocols using DockBench 1.01 [41]. Each ligand was docked 20 times using GOLD using PLP [42] integrated in the virtual screening platform of DockBench. The docking protocol parameters were maintained in accordance with the benchmark study. The stability over the time of the poses was further evaluated by MD simulation in explicit solvent, running three different repetitions of 10 ns each using the ACEMD [43] MD engine coupled to the AMBER12 forcefield [44]. Geometrical stability was assessed by computing the mean RMSD over the three replicas repetitions. The energetic stability of the interaction was evaluated by computing protein-ligand binding affinities by the MMGBSA method [45]. A detailed protocol including the preparation of the system for MD simulation and the parameters of the MD and the MMGBSA calculations was derived from the recently reported pipeline used in Grand Challenge 2 [46] organized by the Drug Design Data Resource Community (drugdesigndata.org), except for the length of the replicas, 10 ns instead 2 ns, and for the time step of 2 fs instead of 4 fs.

Acknowledgements

We are grateful to Dr. Marino Bellini for technical assistance with mass spectrometry analyses. The computational work coordinated by S. Moro, as well as synthesis by M.G. Ferlin, biological evaluation by G. Viola and L. Quintieri, were supported with financial

support from the University of Padova, Italy. The work of M.S. was supported by the University of Padova, Italy (UNIPD, Progetto Giovani Studiosi 2013: Protocol number 79122). Molecular Modeling Section lab is also very grateful to the Chemical Computing Group for its scientific and technical partnership. S. Moro participates in the European COST Action CM1207 (GLISTEN).

Appendix A. Supplementary data Supplementary data related to this article can be found at

Disclaimer

The content of this paper is solely the responsibility of the authors and does not necessarily reflect the official views of the National Institutes of Health.

References

- [1] W.K. Hagmann, The many roles for fluorine in medicinal chemistry, *J. Med. Chem.* 51 (2008) 4359–4369. doi:10.1021/jm800219f.
- [2] E.P. Gillis, K.J. Eastman, M.D. Hill, D.J. Donnelly, N.A. Meanwell, Applications of Fluorine in Medicinal Chemistry, *J. Med. Chem.* 58 (2015) 8315–8359. doi:10.1021/acs.jmedchem.5b00258.
- [3] S. Swallow, Fluorine in medicinal chemistry, in: *Prog. Med. Chem.*, Elsevier, 2015: pp. 65–133. doi:10.1016/bs.pmch.2014.11.001.
- [4] P. Shah, A.D. Westwell, The role of fluorine in medicinal chemistry, *J. Enzyme Inhib. Med. Chem.* 22 (2007) 527–540. doi:10
- [5] *Bioorganic and Medicinal Chemistry of Fluorine*, Jean-Pierre Bégué, Danièle Bonnet-Delpon, Effects of Fluorine Substitution on Biological Properties, chapter

3,11 October 2007, John Wiley & Sons, Inc.

- [6] Parkinson A and Ogilvie BW (2008) Biotransformation of xenobiotics, in Casarett & Doull's Toxicology. The Basic Science of Poisons, 7th ed. (Klaassen CD ed) pp 161–304, McGraw-Hill, New York.
- [7] M.G. Ferlin, G. Palù, G. Chiarelto, V. Pezzi, I. Castagliuolo, V. Gasparotto, L. Barzon, L. Dalla Via, Synthesis and in Vitro and in Vivo Antitumor Activity of 2-Phenylpyrroloquinolin-4-ones, *J. Med. Chem.* 48 (2005) 3417–3427. doi:10.1021/jm049387x.
- [8] V. Gasparotto, I. Castagliuolo, G. Chiarelto, V. Pezzi, D. Montanaro, P. Brun, G. Palù, G. Viola, M.G. Ferlin, Synthesis and biological activity of 7-phenyl-6,9-dihydro-3H-pyrrolo[3,2-f]quinolin-9-ones: a new class of antimitotic agents devoid of aromatase activity., *J. Med. Chem.* 49 (2006) 1910–5. doi:10.1021/jm0510676.
- [9] V. Gasparotto, I. Castagliuolo, M.G. Ferlin, 3-Substituted 7-phenyl-pyrroloquinolinones show potent cytotoxic activity in human cancer cell lines, *J. Med. Chem.* 50 (2007) 5509–5513. doi:10.1021/jm070534b.
- [10] M.G. Ferlin, R. Bortolozzi, P. Brun, I. Castagliuolo, E. Hamel, G. Basso, G. Viola, Synthesis and in vitro evaluation of 3H-pyrrolo[3,2-f]-quinolin-9-one derivatives that show potent and selective anti-leukemic activity, *ChemMedChem.* 5 (2010) 1373–1385. doi:10.1002/cmdc.201000180.
- [11] D. Carta, R. Bortolozzi, M. Sturlese, V. Salmaso, E. Hamel, G. Basso, L. Calderan, L. Quintieri, S. Moro, G. Viola, M.G. Ferlin, Synthesis, structure-activity relationships and biological evaluation of 7-phenyl-pyrroloquinolinone 3-amide derivatives as potent antimitotic agents, *Eur. J. Med. Chem.* 127 (2017) 643–660. doi:10.1016/j.ejmech.2016.10.026.

- [12] R.S. Obach, G.S. Walker, M.A. Brodney, Biosynthesis of fluorinated analogs of drugs using human cytochrome P450 enzymes followed by deoxyfluorination and quantitative nuclear magnetic resonance spectroscopy to improve metabolic stability, *Drug Metab. Dispos.* 44 (2016) 634–646. doi:10.1124/dmd.116.069310.
- [13] S. Ono, T. Hatanaka, H. Hotta, T. Satoh, F.J. Gonzalez, M. Tsutsui, Specificity of substrate and inhibitor probes for cytochrome P450s: evaluation of *in vitro* metabolism using cDNA-expressed human P450s and human liver microsomes, *Xenobiotica.* 26 (1996) 681–693. doi:10.3109/00498259609046742.
- [14] R.S. Obach, Inhibition of human cytochrome P450 enzymes by constituents of St. John's Wort, an herbal preparation used in the treatment of depression., *J. Pharmacol. Exp. Ther.* 294 (2000) 88–95.
- [15] H. Rastogi, S. Jana, Evaluation of inhibitory effects of caffeic acid and quercetin on human liver cytochrome P450 activities, *Phyther. Res.* 28 (2014) 1873–1878. doi:10.1002/ptr.5220.
- [16] R. Romagnoli, P.G. Baraldi, M.K. Salvador, F. Prencipe, V. Bertolasi, M. Cancellieri, A. Brancale, E. Hamel, I. Castagliuolo, F. Consolaro, E. Porcù, G. Basso, G. Viola, Synthesis, antimitotic and antivascular activity of 1-(3',4', 5'-trimethoxybenzoyl)-3-arylamino-5-amino-1,2,4-triazoles, *J. Med. Chem.* 57 (2014) 6795–6808. doi:10.1021/jm5008193.
- [17] M.L. Dupuis, M. Tombesi, M. Cianfriglia, Modulation of the multidrug resistance (MDR) phenotype in CEM MDR cells simultaneously exposed to anti HIV-1 protease inhibitors (PI's) and cytotoxic drugs., *Ann. Ist. Super. Sanita.* 38 (2002) 387–92.
- [18] E. Hamel, Evaluation of antimitotic agents by quantitative comparisons of their effects on the polymerization of purified tubulin, *Cell Biochem. Biophys.* 38 (2003) 1–21.

doi:10.1385/CBB:38:1:1.

- [19] P. Verdier-Pinard, J.Y. Lai, H.D. Yoo, J. Yu, B. Marquez, D.G. Nagle, M. Nambu, J.D. White, J.R. Falck, W.H. Gerwick, B.W. Day, E. Hamel, Structure-activity analysis of the interaction of curacin A, the potent colchicine site antimitotic agent, with tubulin and effects of analogs on the growth of MCF-7 breast cancer cells., *Mol. Pharmacol.* 53 (1998) 62–76. doi:10.1124/mol.53.1.62.
- [20] M. Fujita, K. Ajiro, A. Iwamatsu, H. Goto, T. Okigaki, M. Inagaki, H. Kosako, T. Takahashi, M. Sakurai, K. Okawa, Y. Tomono, Identification of a Novel Phosphorylation Site on Histone H3 Coupled with Mitotic Chromosome Condensation, *J. Biol. Chem.* 274 (2002) 25543–25549. doi:10.1074/jbc.274.36.25543.
- [21] B.A.A. Weaver, D.W. Cleveland, Decoding the links between mitosis, cancer, and chemotherapy: The mitotic checkpoint, adaptation, and cell death, *Cancer Cell.* 8 (2005) 7–12. doi:10.1016/j.ccr.2005.06.011.
- [22] P.R. Clarke, L.A. Allan, Cell-cycle control in the face of damage - a matter of life or death, *Trends Cell Biol.* 19 (2009) 89–98. doi:10.1016/j.tcb.2008.12.003.
- [23] I. Vitale, A. Antocchia, C. Cenciarelli, P. Crateri, S. Meschini, G. Arancia, C. Pisano, C. Tanzarella, Combretastatin CA-4 and combretastatin derivative induce mitotic catastrophe dependent on spindle checkpoint and caspase-3 activation in non-small cell lung cancer cells, *Apoptosis.* 12 (2007) 155–166. doi:10.1007/s10495-006-0491-0.
- [24] C. Cenciarelli, C. Tanzarella, I. Vitale, C. Pisano, P. Crateri, S. Meschini, G. Arancia, A. Antocchia, The tubulin-depolymerising agent combretastatin-4 induces ectopic aster assembly and mitotic catastrophe in lung cancer cells H460, *Apoptosis.* 13 (2008) 659–669. doi:10.1007/s10495-008-0200-2.

- [25] Y. Tsujimoto, S. Shimizu, Role of the mitochondrial membrane permeability transition in cell death, *Apoptosis*. 12 (2007) 835–840. doi:10.1007/s10495-006-0525-7.
- [26] S. Xiong, T. Mu, G. Wang, X. Jiang, Mitochondria-mediated apoptosis in mammals, *Protein Cell*. 5 (2014) 737–749. doi:10.1007/s13238-014-0089-1.
- [27] E. Lugli, L. Troiano, A. Cossarizza, Polychromatic analysis of mitochondrial membrane potential using JC-1., *Curr. Protoc. Cytom. Chapter 7* (2007) Unit7.32. doi:10.1002/0471142956.cy0732s41.
- [28] A. Rovini, A. Savry, D. Braguer, M. Carré, Microtubule-targeted agents: When mitochondria become essential to chemotherapy, *Biochim. Biophys. Acta - Bioenerg.* 1807 (2011) 679–688. doi:10.1016/j.bbabi.2011.01.001.
- [29] R. Romagnoli, P.G. Baraldi, C. Lopez-Cara, D. Preti, M. Aghazadeh Tabrizi, J. Balzarini, M. Bassetto, A. Brancale, X.H. Fu, Y. Gao, J. Li, S.Z. Zhang, E. Hamel, R. Bortolozzi, G. Basso, G. Viola, Concise Synthesis and Biological Evaluation of 2-Aroyl-5-Amino Benzo[b]thiophene Derivatives As a Novel Class of Potent Antimitotic Agents, *J. Med. Chem.* 56 (2013) 9296–9309. doi:10.1021/jm4013938.
- [30] R. Romagnoli, P.G. Baraldi, M.K. Salvador, F. Prencipe, C. Lopez-Cara, S. Schiaffino Ortega, A. Brancale, E. Hamel, I. Castagliuolo, S. Mitola, R. Ronca, R. Bortolozzi, E. Porcuì, G. Basso, G. Viola, Design, Synthesis, in Vitro, and in Vivo Anticancer and Antiangiogenic Activity of Novel 3-Arylamino benzofuran Derivatives Targeting the Colchicine Site on Tubulin, *J. Med. Chem.* 58 (2015) 3209–3222. doi:10.1021/acs.jmedchem.5b00155.
- [31] N. Zamzami, P. Marchetti, M. Castedo, D. Decaudin, A. Macho, T. Hirsch, S.A. Susin, P.X. Petit, B. Mignotte, G. Kroemer, Sequential reduction of mitochondrial transmembrane potential and generation of reactive oxygen species in early

- programmed cell death., *J. Exp. Med.* 182 (1995) 367–77. doi:10.1084/jem.182.2.367.
- [32] J. Cai, D.P. Jones, Superoxide in apoptosis. Mitochondrial generation triggered by cytochrome c loss, *J. Biol. Chem.* 273 (1998) 11401–11404. doi:10.1074/jbc.273.19.11401.
- [33] H. Nohl, L. Gille, K. Staniek, Intracellular generation of reactive oxygen species by mitochondria, *Biochem. Pharmacol.* 69 (2005) 719–723. doi:10.1016/j.bcp.2004.12.002.
- [34] G. Rothe, G. Valet, Flow cytometric analysis of respiratory burst activity in phagocytes with hydroethidine and 2',7'-dichlorofluorescein., *J. Leukoc. Biol.* 47 (1990) 440–448.
- [35] M.E. Harley, L.A. Allan, H.S. Sanderson, P.R. Clarke, Phosphorylation of Mcl-1 by CDK1-cyclin B1 initiates its Cdc20-dependent destruction during mitotic arrest, *EMBO J.* 29 (2010) 2407–2420. doi:10.1038/emboj.2010.112.
- [36] I.E. Wertz, S. Kusam, C. Lam, T. Okamoto, W. Sandoval, D.J. Anderson, E. Helgason, J.A. Ernst, M. Eby, J. Liu, L.D. Belmont, J.S. Kaminker, K.M. O'Rourke, K. Pujara, P.B. Kohli, A.R. Johnson, M.L. Chiu, J.R. Lill, P.K. Jackson, W.J. Fairbrother, S. Seshagiri, M.J.C. Ludlam, K.G. Leong, E.C. Dueber, H. Maecker, D.C.S. Huang, V.M. Dixit, Sensitivity to antitubulin chemotherapeutics is regulated by MCL1 and FBW7, *Nature.* 471 (2011) 110–114. doi:10.1038/nature09779.
- [37] M.D. Haschka, C. Soratroi, S. Kirschnek, G. Häcker, R. Hilbe, S. Geley, A. Villunger, L.L. Fava, The NOXA-MCL1-BIM axis defines lifespan on extended mitotic arrest, *Nat. Commun.* 6 (2015) 6891. doi:10.1038/ncomms7891.
- [38] R. Ronca, E. Di Salle, A. Giacomini, D. Leali, P. Alessi, D. Coltrini, C. Ravelli, S. Matarazzo, D. Ribatti, W. Vermi, M. Presta, Long Pentraxin-3 Inhibits Epithelial-

- Mesenchymal Transition in Melanoma Cells, *Mol. Cancer Ther.* 12 (2013) 2760–2771.
doi:10.1158/1535-7163.MCT-13-0487.
- [39] J.J.P. Stewart, Optimization of parameters for semiempirical methods V: Modification of NDDO approximations and application to 70 elements, *J. Mol. Model.* 13 (2007) 1173–1213. doi:10.1007/s00894-007-0233-4.
- [40] Chemical Computing Group (CCG) Inc. Molecular Operating Environment (MOE);
Chemical Computing Group: 1010 Sherbooke St. West, Suite #910, Montreal, QC,
Canada, H3A 2R7, 2016.
- [41] A. Cuzzolin, M. Sturlese, I. Malvacio, A. Ciancetta, S. Moro, DockBench: An
integrated informatic platform bridging the gap between the robust validation of
docking protocols and virtual screening simulations, *Molecules.* 20 (2015) 9977–9993.
doi:10.3390/molecules20069977.
- [42] GOLD suite, version 5.2 (Internet). Cambridge Crystallographic Data Centre:12 Union
Road, Cambridge CB2 1EZ, UK. Available from: <http://www.ccdc.cam.ac.uk>.
- [43] M.J. Harvey, G. Giupponi, G. De Fabritiis, ACEMD: Accelerating biomolecular
dynamics in the microsecond time scale, *J. Chem. Theory Comput.* 5 (2009) 1632–
1639. doi:10.1021/ct9000685.
- [44] J.A. Maier, C. Simmerling, L. Wickstrom, K.E. Hauser, C. Martinez, K. Kasavajhala,
ff14SB: Improving the Accuracy of Protein Side Chain and Backbone Parameters from
ff99SB, *J. Chem. Theory Comput.* 11 (2015) 3696–3713.
doi:10.1021/acs.jctc.5b00255.
- [45] B.R. Miller, T.D. McGee, J.M. Swails, N. Homeyer, H. Gohlke, A.E. Roitberg,
MMPBSA.py: An efficient program for end-state free energy calculations, *J. Chem.*

Theory Comput. 8 (2012) 3314–3321. doi:10.1021/ct300418h.

- [46] V. Salmaso, M. Sturlese, A. Cuzzolin, S. Moro, Combining self- and cross-docking as benchmark tools: the performance of DockBench in the D3R Grand Challenge 2, J. Comput. Aided. Mol. Des. 32 (2018) 251–264. doi:10.1007/s10822-017-0051-4.

ACCEPTED MANUSCRIPT

HIGHLIGHTS

- A small number of fluoro-phenylpyrroloquinolinones was synthesized
- **12**, and **15** were the best anticancer compounds both *in vitro* and *in vivo*
- **12**, **13** and **15** did not induce significant cell death in normal human lymphocytes
- **12**, **13** and **15** overcame multidrug resistance
- The 3-benzoyl derivatives **15** and **19** showed good metabolic stability in human liver microsomes